Within-field spatial variability of greenhouse gas fluxes from an extensive and intensive sheep-grazed pasture

Alice F. Charteris[a], Paul Harris[a], Karina A. Marsden[b,1], Ian M. Harris[b], Ziwei Guo[a,2], Deborah A. Beaumont[a], Helena Taylor[a], Gianmarco Sanfratello[b,3], Davey L. Jones[b,c], Sarah C. M. Johnson[d], Mick J. Whelan[d], Nicholas Howden[e], Hadewij Sint[a], David R. Chadwick[b] and Laura M. Cárdenas[a]*

[a] Sustainable Agriculture Sciences, Rothamsted Research, North Wyke, Okehampton, Devon, EX20 2SB, UK; [b] School of Natural Sciences, Bangor University, Bangor, Gwynedd, LL57 2UW, UK; [c] UWA School of Agriculture and Environment, University of Western Australia, Perth, WA 6009, Australia; [d] School of Geography, Geology and the Environment, University of Leicester, Leicester, LE1 7RH, UK; [e] School of Civil, Aerospace and Mechanical Engineering, University of Bristol, Bristol, BS8 1TR, UK.

[1] Faculty of Veterinary and Agricultural Sciences, The University of Melbourne, Parkville, Victoria 3010, Australia; [2] School of Civil, Aerospace and Mechanical Engineering, University of Bristol, Bristol, BS8 1TR, UK; [3] Institute of Biological and Environmental and Rural Sciences (IBERS), Aberystwyth University, Aberystwyth, Ceredigion, SY23 3DD, UK.

alice.charteris@rothamsted.ac.uk, paul.harris@rothamsted.ac.uk, k.marsden@bangor.ac.uk, i.m.harris@bangor.ac.uk, zg15273.2014@my.bristol.ac.uk, deborah.beaumont@rothamsted.ac.uk, helena.taylor@rothamsted.ac.uk, gis7@aber.ac.uk, davey.jones@uwa.edu.au, sj239@leicester.ac.uk, mjw72@leicester.ac.uk, nicholas.howden@bristol.ac.uk, hadewij.sint@rothamsted.ac.uk, d.chadwick@bangor.ac.uk, laura.cardenas@rothamsted.ac.uk.

* *Corresponding author:* laura.cardenas@rothamsted.ac.uk

Declaration of competing interests

Declaration of competing interests: The authors have no competing interest to declare.

Abstract

Greenhouse gas (GHG) fluxes from livestock grazed pasture soils are highly variable in both space and time but the quantitative importance of the factors regulating this variation remain poorly understood. Our aim was to explore this variability on contrasting extensively (low input) and intensively managed sheep-grazed 'case-study' pastures. We quantified (through standard and spatially-informed regressions) the statistical relationships between GHG fluxes (nitrous oxide (N_2O), carbon dioxide (CO_2) and methane (CH_4)) and a range of soil, field and management characteristics. Fluxes of these three GHGs at two study sites were highly variable, but spatial structure (i.e. autocorrelation) was only observed in the variability of N_2O fluxes across the intensive site and CO_2 fluxes across the extensive site. The regression analyses identified significant GHG predictor variables for the extensive site as: NO_3^- ($p < 0.001$) and vegetation-type ($p < 0.01$) for N_2O ($R^2 = 0.57$; $p = 0.000$); NH_4^+ ($p < 0.05$), slope ($p < 0.05$) and elevation ($p < 0.01$) for CO_2 ($R^2 = 0.34$; $p = 0.000$); and NO_3^- ($p < 0.01$), NH_4^+ ($p < 0.05$) and soil moisture ($p < 0.05$) for CH_4 ($R^2 = 0.25$; $p = 0.005$). Significant GHG predictor variables for the intensive site were soil moisture ($p < 0.01$) and bulk density ($p < 0.01$) for N_2O ($R^2 = 0.27$; $p = 0.005$); soil moisture ($p < 0.001$) for CO_2 ($R^2 = 0.31$; $p = 0.001$); while none were found for CH_4 ($R^2 = 0.10$; $p = 0.655$). Key factors driving GHG variation were both site- and GHG-specific, with fluxes controlled by local conditions leading to differences in limiting factors (possibly even at the within-site scale). Our statistical analyses suggest a larger range of driving variables (e.g. air and soil temperature or other soil chemical properties such as total extractable N) may be required to more fully capture the observed variability in the GHG processes considered here, and that it may also

be fruitful for future analyses to consider non-linear, non-stationary and interacting relationships across space- and time-scales. Adequacies of each site's sample design also played a key interpretive role in the GHG processes, requiring further evaluation through additional sampling campaigns.

Keywords: upland; lowland; grassland; nitrous oxide; carbon dioxide; methane

1. Introduction

Grazing land is estimated to occupy almost 25% of the Earth's land area (Klein Goldewijk et al., 2017) and plays a substantial and important role in global biogeochemical cycling. Grazing systems are found across the temperate and tropical latitudes and in a wide variety of ecosystems, ranging from managed, irrigated pastures to unmanaged open savannahs and drylands (Asner et al., 2004). In the UK, grazing land occupies over 12 million ha (Office for National Statistics, 2016), and spans extensively managed, unimproved upland grazing areas and intensively managed, improved lowland pastures. This wide range of grazing systems, under differing management intensities and environmental and climatic conditions, provides grazing livestock with differing forages and results in diverse types and degrees of environmental impact.

Within a field, plant and soil characteristics vary in both space and time. Shaw et al. (2016) found that soil ammonium (NH_4^+), nitrate (NO_3^-) and amino acid concentrations varied most over short ranges (< 2 m), but also at larger scales (> 2 m) and was even important at the very small scale (< 1 cm). While soil moisture and temperature, for example, are of course continuously influenced by diurnal and seasonal cycles and weather conditions. Within-field variability is exacerbated by the movement of grazing animals, which results in localised soil compaction and nutrient deposition, and especially so on hill-grazed pastures

where the livestock behaviour is influenced by the heterogeneity of the field, camping for example on small areas of flatter and more sheltered land (Betteridge et al., 2010a,b). The environmental impacts of grazing systems are therefore highly variable within-field, as well as at farm (field-to-field) and landscape (farm-to-farm) scales, making it difficult to generate aggregated estimates of the effects of individual factors.

Agricultural activities are estimated to have contributed 9% of total UK greenhouse gas (GHG) emissions in 2018 (Brown et al., 2020). Methane (CH_4), nitrous oxide (N_2O) and carbon dioxide (CO_2) accounted for 62%, 35% and 3% of these emissions, respectively (Brown et al., 2020). By sector, agriculture currently represents the largest source of total UK CH_4 and N_2O emissions (Brown et al., 2020). The magnitudes of soil-derived N_2O, CH_4 and CO_2 fluxes depend on interactions between a range of fixed and dynamic factors (Giles et al., 2012; Imer et al., 2013; Giltrap et al., 2014; Kaiser et al., 2018). Localised fixed factors include soil texture, structure and bulk density and soil composition, as well as organic matter content, nitrogen (N), carbon (C) and phosphorous (P) availability, cation exchange capacity (CEC) and pH. Broader within field-scale fixed features include a field's aspect, slope and elevation. Dynamic factors encompass previous and prevailing management (including grazing activities and animal behaviour, and perhaps most importantly, urine deposition) and environmental conditions (which feedback to soil characteristics, moisture and temperature). Interactions between factors occur across a range of scales and different processes can occur concurrently in adjacent microsites or predominate over larger areas (Parkin, 1993; Giltrap et al., 2014; Oertel et al., 2016).

Quantifying the spatial and temporal variability of these interactions in grazing systems is critical to improve our understanding of the drivers of N_2O, CO_2 and CH_4 fluxes, enabling better estimates of aggregated GHG emissions and associated uncertainties at the landscape scale (Imer et al., 2013; Giltrap et al., 2014; Cowan et al., 2015). Farm or field-

scale estimates, particularly of N_2O and CH_4, can be skewed (over-estimated) by high fluxes from small areas (hot spots) and/or high fluxes for short periods (hot moments) which happen to coincide with the sampling area(s) or period(s) (McClain et al., 2003; Duncan et al., 2013). Equally, the reverse can be true, and under-estimation can occur if hot spots or hot moments are under-represented during sampling. Furthermore, improved understanding of the spatial and temporal variability of GHG fluxes from different pasture systems will assist with the development of more targeted and efficient mitigation strategies and better aggregated GHG emission estimates and uncertainties for different sites, farms and land use types and with ultimate up-scaling to the national scale.

In this study, we focussed on spatial variability at one time-point. We aimed to assess how a common set of variables drive within-field spatial GHG variability at two different study sites by quantifying the statistically significant relationships between GHG fluxes and soil characteristics and key contextual factors (such as topography, vegetation-type and other nutrient inputs to pastures, e.g. farmyard manure (FYM)). Data were collected using a similar (but appropriately scaled) snapshot sampling approach at the two contrasting (extensively and intensively managed) sheep-grazed field sites. The contribution of sheep-grazed pastures to GHG emissions is less well studied than for cattle (Saggar et al., 2007), despite sheep being globally-important small ruminants which are able to graze a wide range of pastures, including less favourable areas with few alternative agricultural uses (Zervas and Tsiplakou, 2012). For each site, we assess the nature of the spatial autocorrelation (or dependence) in both: (i) the GHG fluxes directly, in respect of a univariate kriging analysis and (ii) the error term of the regression analyses for potentially improved inference in the GHG relationships described.

Practical constraints dictated that the adopted sampling strategies for the different sites could not be identical, and so our study hypotheses were independent and site-specific -

as follows for the two case studies, designed to assess the influence of soil and site parameters on GHG emissions:

A. At the extensively-managed site (Case Study 1), spatial variability of N_2O, CO_2 and CH_4, will each be in part driven by one or more of the following factors: (a) variation in vegetation-type, (b) variation in extractable soil NO_3^-, extractable soil NH_4^+, gravimetric soil moisture content, soil pH, soil percentage water filled pore space (% WFPS), soil bulk density, soil total carbon (% TC), soil total nitrogen (% TN), the TC:TN ratio, soil organic matter and site topography; and (c) spatial autocorrelation effects.

B. At the intensively-managed site (Case Study 2), spatial variability of N_2O, CO_2 and CH_4, will each be in part driven by one or more of the following factors: (a) the boundaries of where FYM was spread; and (b) that listed in (A) parts (b) and (c).

We included two case studies as they represent intensive and extensive grazing management. The wide range of soil and site parameters selected include those typically measured in GHG sampling experiments and known drivers of GHG fluxes. Given the large number of sampling points, it was not possible to conduct some of the more complex or time-consuming analyses, such as soil microbial biomass extractions. Furthermore, some soil and site parameters available to this study will have a certain dependence on each other (i.e. strong correlation) where each will equally explain GHG flux variation. Such parameters were identified in the analyses.

Hypotheses (A) and (B) were tested through a series of regression analyses conducted through a linear mixed model (LMM) framework, preceded by an extensive exploration of the soil, site and GHG flux data and their relationships. For each study site, the drivers of GHG within-field spatial variability were expected to differ due the contrasting characteristics of the two different grazing systems. At each site, the observed GHG variability was partly due to: (1) the known and measured drivers of N_2O, CO_2 or CH_4

available; and (2) the unknown drivers or known drivers that were not measured or available. These were site-specific and, keeping in mind the site-specific sampling strategies, a secondary study aim was to assess likely reasons for observed differences between the different grazing systems. Finally, we also critically assessed the benefits and limitations of the approach taken to explore spatial variability in GHG emissions and suggest avenues for future work.

2. Materials and Methods

2.1. Site descriptions

2.1.1. Extensive management site - Case Study 1

The extensively managed site ('Extensive'; 240-340 m above sea level; a.s.l.) consisted of an 11.5 ha semi-improved, sheep-grazed pasture (Fig. 1; Supplementary Figs. 1, 2) at Bangor University's Henfaes Research Station, Abergwyngregyn, North Wales (53°13'13''N, 4°0'34''W). The field (named Middle Ffridd) has an easterly aspect and a slope of ca. 15%. It had not received inorganic fertiliser or lime, nor had it been re-seeded, in over 30 years. The field is normally stocked with up to 1 Livestock Unit (LU) ha^{-1}, with Welsh Mountain ewes (*Ovis aries*; where each sheep contributes 0.15 LU; Glastir Entry Booklet 2: Technical Guidance 2015, 2013). At the time of the experiment, the stocking rate was 0.39 LU ha^{-1}. The vegetation across the site was composed of a mosaic of 60% bracken (*Pteridium aquilinum*) and 38% semi-improved grassland, with minor areas of marsh/wet flush and gorse (*Ulex europaeus*). The grassland areas were comprised of British NVC classifications U4 (*Festuca ovina – Agrostris capillaris – Galium saxatile* grassland) and MG6 (*Lolium perenne – Cynosurus cristatus* grassland) (Rodwell, 2000). According to FAO (1981), the soil is classified as an Orthic Podzol, with greater amounts of plant litter building up beneath the bracken stands. The bracken was controlled via mechanical treatments twice per year,

ensuring stands do not become too dense or tall. In addition, the above-ground bracken fronds die back over winter months, so grazing animals have the potential to access all areas of the field. The site and its management are typical of an extensively managed hill-grazing site in this area of Wales. The contribution of such sites to GHG emissions has been less well-studied than lowland/intensive pasture sites.

The mean minimum and maximum annual temperatures and mean annual rainfall (1981 to 2010) recorded at the nearest Met Office station, Llanfairfechan (40 m a. s. l.), were 7.6 and 13.7 °C and 1099.7 mm (Met Office). A meteorological station (Skye Instruments Ltd., Llandrindod Wells, UK) was also situated within the field, and in the week preceding sampling (November 2016), air temperatures averaged 5.5 °C (ranging from 2.4 to 10.4 °C) and the mean 10 cm soil temperature was 4.7 °C (3.2 – 6.8 °C). There was only 0.8 mm rainfall (23rd - 29th November 2016) and soil moisture contents were high but declining (ca. 0.62 falling to 0.58 cm^3 cm^{-3} at 5 cm). This corresponded to high pre-sampling % WFPS of ca. 80% at 5 cm and ca. 73% at 10 cm. At the Extensive site soil and gas sampling was conducted on 30th November 2016. On this day the air temperature was slightly cooler at 4 °C than the long-term value for November at 7 °C. No rain was recorded on the sampling day, with the long-term value for November at 5.4 mm.

2.1.2. Intensive management site - Case Study 2

The intensively managed site ('Intensive'; on average 160 m a.s.l.) was a 1.78 ha sheep-grazed pasture (Fig. 1; Supplementary Figs. 3, 4) located in south-west England, at the North Wyke Farm Platform (NWFP), Rothamsted Research, Okehampton, Devon (50°46'10''N, 30°54'05''W). The NWFP is a 63 ha systems-based experimental facility divided into 15 hydrologically isolated sub-catchments across three small farms, used for grazing livestock research (Orr et al., 2016; Takahashi et al., 2018). For this study, we focused on one sub-

catchment which consists of a single field named Dairy North. The field has a northerly aspect, a slope of 10.9% and had been under permanent grassland since the 1990s with *Lolium perenne* as the dominant grass species and minor contributions from *Agrostis stolonifera* and *Holcus lanatus*. It received inorganic fertiliser in the form of ammonium nitrate (NH_4NO_3) at a rate of 160 kg N ha^{-1} as four applications of 40 kg N ha^{-1} per year. The field was grazed by a March-lambing flock of Suffolk x Mule ewes (crossed mainly with Texel or Charollais rams), with 34 animals present up until three days before the sampling was carried out (stocking rate of ca. 2.9 LU ha^{-1}, where one sheep is 0.15 LU). The soil class (Harrod and Hogan, 2008) is Halstow (Gleyic Cambisol; Avery, 1980), which comprises a slightly stony clay loam topsoil (approximately 36% clay) that overlies a mottled stony clay (approximately 60% clay), derived from underlying Carboniferous Culm rocks. The NWFP is managed as a typical farm for the area, evaluating different strategies on the three farm-lets.

The mean annual temperature in North Wyke is approximately 10 °C, the mean annual rainfall (1960-2000) is 1055.7 mm (Harrod and Hogan, 2008) and the climate is classed as cool temperate. In the week preceding sampling (July 2016), air temperatures averaged 15.3 °C (ranging from 10.2 to 21.1 °C) and the mean 10 cm soil temperature was 18.2 °C (14.4 – 22.4 °C). There was only 4.2 mm rainfall in this week (25th - 31st July 2016), spread across approximately ten small events. At the Intensive site soil and gas sampling was conducted on 1st August 2016. On this day the mean air temperature was 14 °C, similar to the long-term value of 15 °C. Rainfall was 12 mm on the sampling day, much higher than the long-term daily value for August of 2 mm.

2.2. Spatial sampling methodologies

2.2.1. Sample locations

At the Extensive site, 112 sampling points were established on a regular grid of 30 m × 30 m

228 across the 11.5 ha, together with three randomly allocated sampling points (giving a total
229 sample size of n = 115). Locations were marked in the field using a GeoXT handheld GPS
230 unit (Trimble Inc., Sunnyvale, CA). The chosen grid resolution was considered to provide
231 reasonable site coverage within the available resources (operators, time and budget) and was
232 not informed by a pilot study (for N_2O, CH_4 and CO_2 fluxes).

233 At the Intensive site, a 15 m × 15 m grid (78 sampling points) combined with an
234 offset 25 m × 25 m grid (21 sampling points) was used to give a total of n = 99 sampling
235 points across the 1.78 ha field. The overlay of two regular sampling grids loosely mimics the
236 effect of a random stratified sampling approach with a 15 m grid and a single point allocated
237 at random within each 15 m grid cell (via the 25 m grid). The strategy was chosen to better
238 capture small-scale spatial variation (i.e. that below 15 m) and benefited from information
239 provided by a pilot study, on a 25 m grid only, for soil inorganic N the previous year (July
240 2015). Again ultimately, the grid resolutions were dictated by available resources. Locations
241 were marked in the field by Real Time Kinematic (RTK) surveying using a Trimble® R6
242 GNSS Receiver and Trimble® R8 base station (Trimble Inc., Sunnyvale, CA). Figure 1
243 depicts the sampling locations at each study site.

244

245 *2.2.2. Soil and greenhouse gas sampling*

246 Air-tight static chambers were employed at both sites for soil headspace gas sampling (De
247 Klein and Harvey, 2012). Smaller cylindrical chambers were used at the Extensive site than
248 at the Intensive site, where cuboid chambers were employed (see Supplementary Information
249 [SI] for chamber design and insertion details and gas sampling strategies). Headspace gas
250 samples were collected immediately after chamber closure (0 min) and again after 60 min at
251 the Extensive site, whilst at the Intensive site initial chamber headspace gas concentrations
252 were approximated by ambient air sampling (Chadwick et al., 2014) and chambers were

sampled 40 min after closure. Two-point headspace sampling was necessary due to the large numbers of chambers to be sampled in a short window, and has been shown to be acceptable under similar site conditions (Chadwick et al., 2014; on average >90% of 1970 chamber measurements fitted a linear function) and linear (or approximately linear) increases in headspace concentrations were anticipated based on substantial work at the sites (SI). By using a team of trained researchers, gas sampling was conducted within a few hours at both sites (Extensive site: 10:40-12:40 h; Intensive site: 10:00-14:00 h), minimising sampling time of day effects. Note that the CO_2 fluxes represent soil and plant respiration without photosynthesis due to the opaque nature of the chambers.

After gas sampling, chamber lids were removed and hand-held temperature probes used (inserted ca. 0-5 cm depth at the Extensive site, and ca. 0-10 cm depth at the Intensive site) to record soil temperature. Chamber heights (four measurements within each chamber) were then recorded in order to calculate chamber headspace volumes. Bulk density cores (100 cm^3, 0-5 cm at the Extensive site; 0-10 cm at the Intensive site) and soil samples (four 0-5 cm cores (bulked) at the Extensive site; six 2.5 cm-diameter, 0-10 cm cores (bulked) at the Intensive site) were taken from within the chamber areas. Bulk density cores and soil samples were stored in polythene bags in refrigerators (at 4 °C) prior to analysis.

2.3. Determination of soil and greenhouse gas parameters

Extensive site soil extractions and pH measurements were conducted within 24 h of sample collection, while analyses for Intensive site samples were completed within 5 days. For each site, the determination of bulk density (termed BD in the statistical summaries, graphics etc.), soil % WFPS (WFPS), extractable soil NO_3^--N and NH_4^+-N (NO_3^-N and NH_4^+N), soil pH (pH), gravimetric soil moisture content (SM), soil organic matter (SOM), soil % TC and % TN contents (TC and TN) are given in detail in SI. Soil headspace GHG concentrations (N_2O,

CO_2 and CH_4, termed N_2O, CO_2 and CH_4, respectively) were determined using the same Perkin Elmer Clarus 580 Gas Chromatograph fitted with an electron capture detector for N_2O measurement and a flame ionisation detector for CO_2 and CH_4 determination for both sites (see SI for further details).

2.4. Topography, vegetation and manure spread data

For each site, elevation (ELEV), aspect (not used) and slope (SLOP) data were calculated utilising 1 m LiDAR grids (see SI for details). The compound topographic index (CTI; Moore et al., 1991; Sørensen et al., 2006; Evans et al., 2014) was also derived from the LiDAR data. For the Extensive site only, a vegetation-type variable (VT) was created consisting of the four vegetation classes: bracken, gorse (but not sampled on), grassland and marsh (only one sample location). Gorse was not sampled as it represented a very small proportion (< 1%) of the site and VT was reduced to three classes. For the Intensive site only, organic FYM was not spread within 2 m of the field boundary (i.e. the hedge or fence), or within 10 m of a watercourse (including French drains); a binary variable (termed OS for "organic spread") was therefore created indicating whether a sample site fell within or outside of the FYM boundary (OS = 1 inside; OS = 0 outside).

2.5. Statistical methods

In this study, the following regressions in both non-spatial and spatial forms were fitted, for the Extensive and Intensive sites, respectively:

$$\left.\begin{matrix} N_2O \\ CO_2 \\ CH_4 \end{matrix}\right\} = f(NO_3^-N + NH_4^+N + pH + SM + WFPS + BD + TC + TN + CNR + SOM + SLOP + ELEV + CTI + VT)$$

Equation 1

$$\left.\begin{matrix} N_2O \\ CO_2 \\ CH_4 \end{matrix}\right\} = f(NO_3^-N + NH_4^+N + pH + SM + WFPS + BD + TC + TN + CNR + SOM + SLOP + ELEV + CTI + OS)$$

Equation 2

where CNR is the TC:TN ratio. Thus, in total, twelve regressions (the non-spatial and spatial forms, for the three GHGs, at the two sites) were considered where the GHG response variables of N_2O, CO_2 and CH_4 fluxes were related to predictor variables measuring soil properties (NO_3^-N, NH_4^+N, pH, SM, WFPS, BD, TC, TN, CNR and SOM), topography (SLOP, ELEV and CTI) and site-specific pasture characteristics (VT or OS). The predictors were treated as fixed effects. Although available, soil temperature data was not included as a predictor variable as data were very similar across each site due to the 'snapshot' nature of the study. Aspect was not included because a preliminary analysis indicated very weak correlations with the GHGs. Interaction terms (predictors) were not considered (e.g. such as NO_3^-N x SM for the N_2O regression). The regressions were fitted through an LMM framework, preceded by a series of exploratory analyses for a richer understanding of the GHG processes.

2.5.1. Exploratory analyses

In the first instance, basic descriptive statistics (mean, standard error of the mean and standard deviation), robust (outlier-resistant) descriptive statistics (median, Qn-scale estimator) and histograms, were used to explore the Extensive and Intensive site data, for each soil, topographic and gas parameter in turn. Secondly, a spatial autocorrelation analysis was undertaken through the calculation of variograms to determine the strength of spatial

dependence in the N_2O, CO_2 and CH_4 fluxes. The valid observation of spatial autocorrelation effects is dependent on: (a) whether or not they actually exist in the data and (b) whether or not the two sample designs are sufficient for these effects to be reliably captured. Important scales of spatial autocorrelation can go un-noticed through poor sample design (e.g. Webster and Lark, 2012). Thirdly, the N_2O, CO_2 and CH_4 fluxes were each investigated over the Extensive and Intensive sites, through six independent (univariate only) geostatistical prediction analyses to a grid. Specifically, the Empirical Maximum Likelihood Kriging (EMLK) algorithm of Pardo-Igúzquiza and Dowd (2005a; 2005b) was used, whose variogram parameters were estimated by Restricted Maximum Likelihood (REML; Ribeiro and Diggle, 2001), to normal scores transformed data. Details of EMLK are given in SI. Fourthly, and to complete the exploratory analyses, an assessment of data relationships was undertaken through scatterplots and linear correlation coefficients (for relating the GHGs to the continuous data – i.e. soils and topography) and conditional boxplots (for relating the GHGs to the categorical/indicator data – i.e. vegetation-type and OS). Unlike SLOP, ELEV, CTI, VT and OS, which are all exhaustive and available throughout the pasture, the sampled nature of the soil-based predictors (NO_3^-N, NH_4^+N, pH, SM, WFPS, BD, TC, TN, CNR, SOM) prevents their use for the GHG prediction surfaces (i.e. extending EMLK to a multivariate form (Hengl et al., 2003) to produce prediction grids or 'heatmaps'), unless the soil-based predictors are exhaustively sampled.

2.5.2. Non-spatial and spatial multivariate regression analyses

Study multivariate regressions (Eq. 1 and Eq. 2) were constructed in six non-spatial and six spatial forms, where the parameters of the former were estimated through ordinary least squares (OLS), while the parameters of the latter were estimated through REML, to unbiasedly account for a spatially-autocorrelated error term (as modelled by a residual

variogram). As in the EMLK analyses, initial starting parameters for the variogram component of the (iterative) REML fits were found using (biased) parameters from a weighted least squares (WLS) variogram model fit to the corresponding empirical variogram. The OLS- and REML-estimated regressions were conducted using LMM functions in the R nlme package (Pinheiro et al., 2018). Again, as in the EMLK analyses, only isotropic exponential variogram models were considered, but now to characterise spatial dependence in residual data. To promote linearity in regression relationships, Box-Cox transforms (Box and Cox, 1964) were used to transform both the response (gases) and predictor (soils, topography, class) variables, where appropriate. Regression outcomes were reported through model parameter significance tests together with R^2, Akaike Information Criterion (AIC) and Bayesian Information Criterion (BIC) model fit summaries. AIC and BIC account for model complexity and model prediction accuracy, whereas R^2 values only reflect the latter[1].

For interpretation of the regressions, note that WFPS is a function of soil moisture and bulk density, CTI is a function of slope and elevation (and also aspect), and soil TC and TN are represented in addition to their ratio (as recommended by Kronmal, 1993). Such dependencies in the predictor variable data sets may create unwanted collinearity effects, in addition to likely collinearities between say, TC and SOM, and therefore may mask important drivers of GHG variability. In this respect, variance inflation factors (VIFs) for each predictor in the regressions were calculated and predictors with a VIF > 10 were removed (following guidelines given in Belsley et al., 1980; O'Brien, 2007) and the regression re-fitted. An alternative to improve statistical inferences in the presence of collinearity can be found in a penalised regression (e.g. Zou and Hastie 2005) but was not considered in this instance.

[1] Reporting of an R^2 value for REML regressions should be viewed cautiously as R^2 is designed for an OLS fit and as such, does not account for error variation due to residual spatial autocorrelation. Thus, *p*-values for R^2 significance are only reported for OLS regressions. However, all such tests of significance themselves can only be viewed as indicative when the assumptions of data independence are not met (as is common with spatial data). This is similarly true for reporting the significance for *r* values.

373

374 *2.5.3. Data truncation for outlying CH_4 values*

375 For the Extensive site data, one relatively high CH_4 flux consistently stood out as outlying in
376 a univariate (via the histogram), bivariate (via scatterplots) and 'distance-paired' (via the
377 variogram) sense. It was decided, therefore, to truncate this flux to the next flux in the
378 ordered data set, plus 20% of that next flux. Thus, a CH_4 flux of 253.81 μg CH_4-C m^{-2} h^{-1} was
379 truncated to 25.15 μg CH_4-C m^{-2} h^{-1}. Similarly, for the Intensive site data, two CH_4 fluxes
380 stood out as outlying and were truncated; one relatively low at -82.29 μg CH_4-C m^{-2} h^{-1}
381 (truncated to -52.14 μg CH_4-C m^{-2} h^{-1}) the other relatively high at 662.71 μg CH_4-C m^{-2} h^{-1}
382 (truncated to 275.85 μg CH_4-C m^{-2} h^{-1}). Data truncation decisions are common to many
383 statistical studies (e.g. Costa, 2014) and provide a pragmatic solution to the use of a more
384 involved robust, non-linear statistical analysis (e.g. through the use of copulas, following
385 Kazianka and Pilz, 2010), when only a few observations are outlying. A sensitivity analysis
386 (not shown) to the three data truncations resulted in no obvious adverse consequences to the
387 resultant statistical interpretations of the Extensive and Intensive site CH_4 spatial processes.
388 The locations of the three data truncations are shown in the CH_4 maps of Figure 2 (one of
389 which is near the field entrance of the Intensive site).

390

391 **3. Results and Discussion**

392 ***3.1. Soil properties and site topography***

393 To provide an understanding of the conditions under which the GHGs were produced,
394 descriptive statistics for the soil variables recorded on one sampling date for each site and
395 each site's topography are shown in Table 1. The Extensive site soil and topographic
396 parameters measured were consistent with other site characteristics described in section 2.1.1.
397 In accordance with the organic matter inputs to the upper soil layers at the Extensive site and

398 the podzolic soil type (Harrison & Bocock, 1981), soil bulk density was low at some
399 sampling points (minimum of 0.34 g cm^{-3}) and below typical values for mineral soils on
400 average (median 0.55 g cm^{-3} cf. ca. 1.3 g cm^{-3}; USDA, 2008). Similarly, SOM was high
401 (median 19%; Ball, 1964) and the soil at the Extensive site was acidic (median pH 4.93),
402 potentially slowing organic matter degradation and inhibiting nitrification (USDA, 2011).
403 The Intensive site had high extractable soil NO_3^- concentrations at some sampling
404 points (up to 237 mg NO_3^--N kg^{-1}), consistent with the regular fertilisation and high livestock
405 stocking rate (Genever and Buckingham, 2016; Baron et al., 2001). Extractable soil NH_4^+
406 concentrations were also high at some sampling points (maximum 146 mg NH_4^+-N kg^{-1}),
407 commonly at the same sampling points at which soil NO_3^- concentrations were particularly
408 high. However, extractable soil NO_3^- and NH_4^+ concentrations were non-normal with a
409 positive skew with the mean concentrations > median concentrations (Table 1).
410
411 ***3.2. Context and spatial variability of the GHG data***
412 *3.2.1. GHG distributions*
413 Emissions of all three GHGs assessed on the sampling date at the Extensive site (Table 2)
414 were comparable to those previously reported at the same site in a year-long automated
415 chamber study by Marsden et al. (2018). Extensive site median N_2O emissions during the
416 growing season from extensively managed pastures at 200 m a.s.l. in Scotland and at 450 m
417 a.s.l. in Switzerland were also similar (4.5 μg N_2O-N m^{-2} h^{-1} here, cf. ca. 6 μg N_2O-N m^{-2} h^{-1}
418 and 1.2 μg N_2O-N m^{-2} h^{-1}, respectively; Flechard et al., 2007). However, for our spatial
419 investigation, greater ranges in N_2O and CH_4 emissions were measured than in Marsden et al.
420 (2018), suggesting that spatial variability exceeds temporal variability at the site, which has
421 also been observed elsewhere (McDaniel et al., 2017). Extensive site N_2O and CO_2 emissions
422 were positively skewed (Fig. 2A) likely due to grazing hotspots (Velthof et al., 1996;

Chadwick et al., 2014; Giltrap et al., 2014; Cowan et al., 2015) and the small chance of directly sampling a recent urine patch. For CH_4, equivalent weak sink behaviour has been previously reported at extensive upland pastures (Imer et al., 2013; Kaiser et al., 2018).

The range of emissions of all three GHGs on the sampling date at the Intensive site was relatively large (Table 2), as observed elsewhere (Turner et al., 2008; Parkin and Venterea, 2010; Jones et al., 2011; Imer et al., 2013; Kaiser et al., 2018). Daily N_2O emissions from a field nearby the lowland site were up to ca. 75 μg N_2O-N m^{-2} h^{-1} in summer (Cardenas et al., 2016), considerably lower than the maximum N_2O emissions observed in this study (216 μg N_2O-N m^{-2} h^{-1}; Table 2). This could be explained by the larger rainfall experienced in our study compared with the long-term value as reported in section 2.2.2. However, a comparable spatial snapshot study (Cowan et al., 2015) conducted on an intensively managed grassland in Scotland in summer (but with grazing sheep remaining in the field during gas measurements) recorded N_2O fluxes with a very similar range (2 to 227 μg N_2O-N m^{-2} h^{-1}) and similar arithmetic and geometric means (25 and 13 μg N_2O-N m^{-2} h^{-1}), as were observed in this study. These high maximal N_2O fluxes likely result from directly sampling of a recent urine patch (sheep were only removed 3 days prior to the experiment at the Intensive site). Correspondingly, Intensive site N_2O and CH_4 fluxes also exhibited positive skew (Fig. 2B), likely again due to antecedent urine patches (Velthof et al., 1996; Chadwick et al., 2014; Giltrap et al., 2014; Cowan et al., 2015). Intensive site CH_4 emissions were consistent with the mixture of sink and source behaviour reported by Cardenas et al. (2016) and Saggar et al. (2007), but slightly weaker maximum sink behaviours were observed in these older studies (ca. -20 and -17 μg CH_4-C m^{-2} h^{-1}, respectively, in summer).

Average GHG fluxes captured in these spatial studies were representative compared with the published literature. However, greater ranges in fluxes were found at both sites than

448 previously recorded in: i) temporally focused emission factor studies at the same sites and; ii)
449 in spatial studies at other sites. For the first point, this likely relates partly to the larger
450 number of independent chambers used, the commonly larger variability of spatial fluxes
451 compared with temporal (McDaniel et al., 2017), and temporal studies may not capture the
452 range of GHG fluxes. The second comparison is likely caused partly by differences in
453 whether, or for how long, grazing livestock are excluded from sites prior to sampling (which
454 in turn influences spatial variability, i.e. point i), and is not consistently handled/reported in
455 the literature). Greater consideration of the impact of antecedent grazing effects is
456 recommended in Charteris et al. (2020) and would aid comparison between studies.
457
458 *3.2.2. GHG spatial dependencies*
459 The normal score variograms (empirical, WLS model and REML model) for
460 Extensive site N_2O, CO_2 and CH_4 data (Table 3; Fig. 3A) on the sampling date all indicated
461 some degree of spatial dependence. However, the Extensive site CH_4 variogram was
462 essentially flat with a relatively high nugget variance, indicating a tendency to random
463 behaviour (as given by the CH_4 sample variance). A relatively high nugget variance was also
464 observed for the Extensive site N_2O variogram, but where a spatial correlation range of 240.0
465 m suggested overall spatial structure. High nugget variances reflect either a true variation in
466 GHG fluxes over short distances or could indicate that the sample design was inadequate to
467 capture small-scale variation. Previous studies have similarly observed limited, or no spatial
468 dependence in N_2O fluxes dependent given the scale of observation (Giltrap et al., 2014).
469 Extensive site CO_2 fluxes displayed clearer spatial structure with a range of 205.2 m, coupled
470 with a smaller nugget than structural variance.
471 Normal score variograms for the GHG data from the Intensive site (Table 3; Fig. 3B)
472 on the sampling date indicated spatial structure was strongest for N_2O, which had a range of

spatial dependence of 82.5 m. Turner et al. (2008) reported N_2O spatial dependence ranges of up to 73 m and 51 m at a dairy grassland in Australia in summer and autumn, while no spatial structure in N_2O fluxes was found in the comparable study at an intensively managed Scottish sheep pasture in summer (Cowan et al., 2015), with a similar mean and range in N_2O fluxes already compared with our Intensive site. The Intensive site CO_2 and CH_4 variograms had relatively high nugget variances, coupled with spatial dependencies of 80.2 m and 84.7 m, respectively. Similar limited spatial dependency has also been reported for CO_2 at a similar site – during 22 sampling events over the course of a year, Kreba et al. (2013) found spatial dependence ranges of between 3.2 m and 70.4 m for a mown, fertilised grassland (at 300 m a.s.l.).

3.2.3. GHG spatial surfaces

The EMLK surfaces for the Extensive and Intensive site GHG predictions on the respective sampling dates, the corresponding 95% prediction credible intervals (PCIs), and the corresponding risk of exceeding a pre-specified threshold (taken as the 80th percentile of the actual, sampled GHG data[2]) are given in Figures 4 and 5. The spatial characteristics of each EMLK surface directly reflect the characteristics of the GHG data as mapped in Figure 2 and the characteristics of the normal scores REML variograms, as given in Table 3 and Figures 3A and 3B. The surfaces also, in part, reflect the kriging neighbourhood specification, where all EMLK runs were specified with at least 33% of nearby data within a minimum distance of 80% of the maximum distance possible, for each grid point GHG prediction (where the prediction grid is approximately at a 0.5 m x 0.5 m resolution).

Given the observed spatial structures and kriging specifications, above, all prediction surfaces resulted in the GHG data being highly smoothed. Uncertainty in the predictions via

[2] The use of the 80th percentile of the sample GHG data is arbitrary and is used for demonstration purposes only. If a recognised widely-approved threshold exists for a given GHG, then it should be used instead.

497 the 95% PCIs, directly relay the variability reflected in the respective variograms, where
498 relatively high nugget variances and high nugget effects (Table 3) were observed. The
499 uncertainty measures via the 95% PCIs were too wide to be of any practical use. Unusually
500 high or low fluxes (hot or cold spots, Figs. 2, 4, 5) did not particularly match any identifiable
501 features in either case study field. Tentatively, it appears that fluxes at the Extensive site
502 tended to be higher around the edge of the field. A tenuous link could be made to sheep using
503 the field boundaries for shelter (i.e. causing nutrient enrichment etc. in these areas - a similar
504 tentative visual spatial pattern was observed in the soil N data, not shown), but only the
505 eastern field boundary had a solid wall that could provide shelter (depending also on the
506 prevailing wind direction), all other field boundaries were wire fences. Intensive site GHG
507 fluxes tended to be higher in an East-West band across the middle of the field, aligning with
508 the field's topography (which is more formally assessed, below). Interestingly, the Intensive
509 site CO_2 surfaces (Fig. 5B) depicted areas of high prediction uncertainty that corresponded to
510 areas of low predicted fluxes, and vice-versa. This was contrary to the other five GHG
511 surfaces, and contrary to what is commonly found in the environmental sciences, where the
512 mean commonly scales proportionally with the variance (Chilès and Delfiner, 1999). The
513 spatial characteristics of the risk of exceedance surfaces reflect chosen thresholds, together
514 with the corresponding prediction/PCI surfaces.
515
516 ***3.3. Soil, topography and other parameters as predictors of GHG fluxes***
517 *3.3.1 Correlation analysis*
518 As further exploration prior to this study's regression fits, the paired relationships
519 (correlations) between the Extensive and Intensive site N_2O, CO_2 and CH_4 fluxes on the
520 relevant sampling date with the pasture soils and topography are presented in Figure 6. The
521 GHG relationships with vegetation-type and OS are given in Figure 7. In the Extensive site

522 case, N_2O, CO_2, soil NO_3^-, soil NH_4^+ and soil moisture were each transformed to
523 (approximate) normality using the Box-Cox transform. In the Intensive site case, N_2O, CH_4,
524 soil NO_3^-, soil NH_4^+ and soil moisture were Box-Cox transformed. Relationships worth
525 highlighting are described as follows, where all highlighted correlations were significant at
526 the 95% level.

527 Extensive site N_2O fluxes were found to be positively correlated with soil NO_3^- (r =
528 0.58), and vegetation-type could, in part, discriminate across the Extensive site N_2O fluxes.
529 For CO_2 fluxes at the same site, weak positive correlations were present with soil NO_3^- (r =
530 0.26) and with soil NH_4^+ (r = 0.32), while a weak negative correlation existed with TC:TN (r
531 = -0.32). For CH_4 fluxes, no relationships were strong enough to warrant highlighting.

532 Intensive site N_2O displayed a weak positive correlation with soil moisture (r = 0.28),
533 a weak negative correlation with elevation (r = -0.30), and OS could have influenced these
534 fluxes. For Intensive site CO_2 fluxes, a moderate positive correlation was present with soil
535 moisture (r = 0.47), a weak positive correlation was present with % WFPS (r = 0.29) and a
536 weak negative correlation was present with elevation (r = -0.28). There were no clear
537 relationships with Intensive site CH_4 fluxes.

538 For correlations between predictor variables, % TC was strongly correlated with %
539 TN for both sites (r = 0.94 and r = 0.95, respectively) and as such, % TC was removed to
540 avoid detrimental collinearity effects before subsequent regressions (i.e. avoid inaccurate
541 coefficient estimation and associated uncertainties). Furthermore, on investigation of the
542 VIFs from initial OLS regressions, it was found that the removal of WFPS (for both sites)
543 ensured all VIFs < 10 (specifically, all VIFs < 2 and < 6 for the extensive and intensive sites,
544 respectively). Thus, detrimental collinearity effects due to the inclusion of WFPS in the
545 regressions were also addressed.
546

3.3.2 Regression analysis

The non-spatial (OLS) and spatial (REML) regression fit summaries for the relevant sampling dates are given in Table 4 (Extensive site) and Table 5 (Intensive site), together with the corresponding (empirical, WLS model and REML model) residual variograms (Figs. 3C, D). As is often the case in a multivariate spatial analysis, structure found in the response variable variograms (as effectively given in Figs. 3A, B) reduces when variance in the response is usefully informed by a set of predictors (in this instance, the soil data, topography etc.). This effect was evident in Figures 3C and 3D, where four of the six residual variograms displayed a random (regression) error structure. Thus, the regressions for Extensive site N_2O and CH_4, and Intensive site CO_2 and CH_4, did not warrant a spatially-autocorrelated error term.

Here, the significant predictors (at least at the 95% level) for Extensive site N_2O regression ($R^2 = 0.57$; $p = 0.000$) were soil NO_3^- and grassland and marsh vegetation-type, while the significant predictors for Extensive site CH_4 regression ($R^2 = 0.25$; $p = 0.005$) were soil NO_3^-, soil NH_4^+ and soil moisture. The significant predictors for Extensive site N_2O regression concur with those recorded as significant in other studies on intensively managed pastures (soil moisture content, NO_3^- and NH_4^+ – Velthof et al., 1996; NO_3^-, NH_4^+ and Olsen-phosphorus – Turner et al., 2008; NO_3^-, pH and % WFPS – Cowan et al., 2015). That NO_3^- was a significant predictor of N_2O emissions across these studies accords well with its substrate role in N_2O production via denitrification and potential limitation due to extensive management and lack of fertilisation at the Extensive site. For CH_4, other studies have found the key predictors of CH_4 to be soil moisture (which commonly leads to relationships with topography; Imer et al., 2013; Kaiser et al., 2018) and % TC content (McDaniel et al., 2017). Methanogenesis is an anaerobic process (increased soil moisture can reduce O_2 availability) which can use small C-containing compounds, as well as CO_2, as substrates which likely

572 explains these relationships. The observed driving effects of soil NO_3^-, soil NH_4^+ on
573 Extensive site CH_4 fluxes are unexplained, but it is important to note that the fit of the
574 Extensive site CH_4 regression was relatively weak, so this should not be over-interpreted. The
575 significant predictor for Intensive site CO_2 regression ($R^2 = 0.31$; $p = 0.001$) was soil
576 moisture only (intercept aside), while no significant predictors were found for Intensive CH_4
577 regression ($R^2 = 0.10$; $p = 0.655$). Soil moisture (important for microbial activity) is a known
578 controlling factor of CO_2 (Kreba *et al.*, 2013), which aligns with its significance in the
579 Intensive site CO_2 regression.

580 Structure in the residual variogram for Extensive site CO_2 was present, but tenuous
581 (Fig. 3C) and this was reflected by only a small decrease in AIC from the non-spatial to the
582 spatial regression (315.7 to 313.6; Table 4) coupled with a slight increase in BIC (357.5 to
583 358.0; Table 4). Unsurprisingly, the non-spatial and spatial regression results for Extensive
584 site CO_2 were broadly similar and the significant predictors were (the intercept), soil NH_4^+,
585 slope and elevation in both cases (noting that the significance of all predictors reduced when
586 spatial effects were included). The R^2 of both the non-spatial and spatial regressions was 0.34
587 (with $p = 0.000$ for the OLS fit). In the literature, CO_2 relationships to soil factors have been
588 various (Kreba et al., 2013) and there are no clear explanations for the significant predictors
589 of Extensive site CO_2.

590 Thus, a REML-based, spatial regression fit was only fully warranted for Intensive site
591 N_2O production (i.e. clear residual variogram structure was evident (Fig. 3D), coupled with
592 sufficient reduction in AIC (360.4 to 354.2 in Table 5) from the non-spatial, OLS-based fit).
593 Here, the significant predictors in the non-spatial regression were soil moisture, soil NO_3^- and
594 elevation, the latter two of which when mapped (the soil NO_3^- map is not shown, but the
595 elevation map is given in Fig. 1B) displayed a clear spatial trend south to north. However, the
596 same two N_2O predictors became insignificant when spatial effects were implicitly catered

for in the regression (via the error term), where now (the intercept), soil moisture (with increased significance) and bulk density were significant predictors of N_2O instead. This critical observation ably demonstrates the importance of accounting for spatial effects for data and processes that are inherently spatial, else incorrect scientific inferences can result (e.g. Harris, 2019). Here correlation should not be confused with causation, but although soil NO_3^- may be considered a driver of N_2O, its weak correlation with N_2O (r = -0.02 from Fig. 6B) suggests the non-spatial regression provides spurious outputs. The R^2 values for these regressions were relatively weak at 0.27 (with p = 0.005 for the OLS fit).

Our hypotheses that one or more of the factors tested drove spatial variability in emissions (and were site-specific) were correct for all GHGs, except Intensive CH_4. However, the fit of the final six regressions ranged from moderately strong to very weak with R^2 values of 0.57, 0.34 and 0.25 for Extensive and 0.27, 0.31 and 0.10 for the Intensive site N_2O, CO_2 and CH_4 fluxes, respectively. Thus, in each instance, as also hypothesised, there are likely missing predictors of N_2O, CO_2 or CH_4, not assessed in this work. These missing predictors could include soil microbial biomass and community composition (for all three GHGs), air temperature, soil temperature (especially for CO_2, see Imer et al., 2013; Kreba et al., 2013), soil electrical conductivity (especially for CH_4, see McDaniel et al., 2017), volumetric water content, porosity, total dissolved N, total extractable N, total dissolved organic carbon, soil hydroxylamine (especially for N_2O, see Liu et al., 2016), distance-based predictors (such as distance from sample site to fence, gate or water trough), un-observed management effects, together with predictors that reflect underlying plant (e.g. root and shoot biomass, likely affecting CO_2 emissions) and livestock emissions (e.g. average sheep movement patterns, spatial intensities of urination). In addition, as already noted in Section 3.2.2., insufficient resolution of spatial sampling could affect the applicability of spatial analyses.

622

623 ***3.4. Comparison of case studies***

624 There are clearly some differences between the two case studies presented in this work that
625 obfuscate their direct comparison (season and weather conditions; site size and management
626 strategies; necessary scaling of sampling resolution between sites; slightly different static
627 chamber designs). In particular, the 10 °C difference in temperature (Extensive: ca. 5 °C vs.
628 Intensive: ca. 15 °C) between the sites is likely to have increased emissions at the Intensive
629 site compared with the Extensive. However, as with the discussion of the results from each
630 site in the context of other published studies in the literature, some cursory comparison is of
631 value. Consistent with the site management (Extensive vs. Intensive), season (autumn vs.
632 summer), lower median extractable soil NO_3^- concentrations (2.0 cf. 6.8 mg NO_3^--N kg^{-1}) and
633 lower median soil pH (4.93 cf. 5.72; Table 1), as well as the lower temperatures, median N_2O
634 fluxes at the Extensive site were lower than those at the Intensive site (4.5 cf. 19.2 μg N_2O-
635 N m^{-2} h^{-1}; Table 2; Flechard et al., 2007; Imer et al., 2013; Marsden et al., 2018; Marsden et
636 al., 2019). Soil moisture content, elevation and NO_3^- concentrations were the significant
637 predictors of N_2O at the Intensive site, while when the appropriate spatially informed
638 regression was used for the Intensive site, NO_3^-, which displayed a clear spatial trend from
639 south to north, was no longer a significant predictor of N_2O (instead these were soil moisture
640 and bulk density only, as elevation also became insignificant). Extractable soil NO_3^-
641 concentrations could also have been less important at the Intensive site as soil concentrations
642 were higher and NO_3^- may not have been a limiting factor in denitrification at this site.
643 Higher extractable soil NO_3^- concentrations at the Intensive site (Table 1) were likely due to
644 considerably higher reactive N inputs per ha – relatively high stocking density (2.9 LU ha^{-1})
645 leading to higher grazing returns, FYM inputs and regular NH_4NO_3 applications. Lower
646 extractable soil NH_4^+ concentrations despite these inputs (median 3.1 cf. 11.4 mg NH_4^+-N kg^-

^{1} at the Extensive site), may have been due to higher crop uptake and/or nitrification rates in the Intensive site soil (Booth et al., 2005) and/or because extractable NH_4^+ was protected from nitrification by organic matter in the Extensive site soil (Cardenas et al., 2013). In addition, nitrification rates at the Extensive site could have been inhibited by the lower soil pH (Table 1; Marsden et al., 2019).

Median CO_2 fluxes were similarly lower at the Extensive site (29.4 cf. 200.5 mg CO_2-C m^{-2} h^{-1}; Table 2), most likely due to the lower temperatures during sampling at this site (Fang and Moncrieff, 2001). A link could be made between the topographic predictor variables of Extensive site CO_2 fluxes (slope and elevation) and the soil moisture predictor at the Intensive site, as topographic parameters can affect soil moisture distributions. However, soil moisture at the Extensive site did not correlate with slope or elevation (Fig. 6), so in this case, significant topographical factors have not acted as surrogates to soil moisture.

Interestingly, at the time of sampling, the Extensive site was on average a CH_4 sink, while the Intensive site was a small source (median: -28.0 cf. 0.3 μg CH_4-C m^{-2} h^{-1}; Table 2). This is despite similar % WFPS values between the sites (52 cf. 57%; Table 1), which, via O_2 availability, is one of the most important controls determining the balance of CH_4 (and N_2O) production and uptake (Imer et al., 2013; Oertel et al., 2016). Imer et al. (2013) found a similar increased likelihood of CH_4 sink behaviour with altitude but hypothesised that this was because the long winter period could not be sampled at the highest altitude site of their study, which would not apply here.

3.5. *Limitations and extensions*

Clearly, the characterization of GHG spatial processes for sheep-grazed ecosystems are a challenge. GHG-generating soil processes vary at the intra-aggregate, microsite scale, upwards to local soil conditions, vegetation type, and topography (centimetre-to-metre scale)

672 and further to soil and ecosystem type (kilometre scale) and beyond (Butterbach-Bahl et al.,
673 2013; Giltrap et al., 2014; Shaw et al., 2016). Adequately capturing such scales of variation is
674 difficult and this was not the direct intention of this study's sample design, where the focus
675 was on estimating spatial dependence effects with respect to assessing key drivers of GHG
676 variability (i.e. the regression models). However, better capturing spatial variability (as for
677 the pilot-informed Intensive site sampling) does improve ability to determine spatial
678 dependence. Sources of GHGs also include GHG-generating plant processes and those
679 associated with the sheep themselves (requiring their movement/behaviour to be captured, see
680 Decandia et al., 2018), neither of which were directly studied here. Furthermore, the
681 influence of the soils, the plants and the livestock on fluxes will differ and interact in a
682 specific manner for each GHG (N_2O, CO_2 and CH_4).
683 We focused on one sampling day for each site as our focus was the within-field
684 spatial variation, not the temporal variation. A single spatial study can only provide a
685 snapshot of GHG variability in time but complements studies that have focused on temporal
686 GHG variation. Notable differences in N_2O outputs between studies can result from
687 differences in the duration of sheep exclusion from the study pasture prior to commencement
688 of the sampling (grazing legacy effects). Given the relative complexity of the factors driving
689 GHG fluxes spatially, spatial GHG variability tends to be larger than temporal GHG
690 variability (McDaniel et al., 2017). Understanding temporal GHG variation is equally
691 important as understanding spatial GHG variation, where for example, the sink/source
692 behaviour of CO_2 is dependent on seasonal weather conditions (Soussana et al., 2007; Mudge
693 et al., 2011; Rutledge et al., 2015; Gourlez de la Motte et al., 2016). Ultimately, it is the
694 characterisation of the full spatio-temporal GHG process that is the research goal. Spatial-
695 only and temporal-only studies are always limited in this respect. A key challenge is
696 advancing sensor technology to measure the GHGs concurrently in space and time, where the

act of measurement itself does not compromise the grazing behaviour of the sheep. Placing chambers in the field compromises grazing behaviour, while eddy covariance cannot capture the spatial detail given it provides an area measurement (i.e. a footprint) and is not well suited to use on hill slopes. Eddy covariance data modelling to characterise spatio-temporal GHG processes from grazing is also inherently involved, requiring suitable expertise to develop, calibrate and interpret.

Some steps towards this goal have been reported. Lush et al. (2018) used tri-axial accelerometers and random forest modelling to identify urination events by grazing sheep, which, when combined with high-resolution GPS movement data, could be used to provide the spatio-temporal distribution of urine patches for the improved estimation of pasture GHG emissions. A combination of eddy covariance and short periods of animal confinement within specific small areas has been used to assess the contribution of cattle to intensive pasture CO_2 and CH_4 emissions (Jérôme et al., 2014; Dumortier et al., 2017). Various new techniques have been developed in recent years to identify urine patches, for example: LiDAR, via grass growth/increased height (Roten et al., 2017); remotely piloted aircraft systems (RPAS) and visible and near infra-red (NIR) imaging, via colour differences (Maire et al., 2018); and Spikey-R technology which measures on soil electrical conductivity (Jolly et al., 2019). Further work is needed, however, to assess the dynamics between patch emission and grass growth to understand the utility of the approach for investigating urine patch-derived GHG hotspots/moments (i.e. growth could be identified one week after urine application, but by this time N_2O emissions may have peaked and diminished). In addition, emission factor trials at UK upland extensively managed sites (Marsden et al., 2018; Marsden et al., 2019) indicate that urine patches do not always act as strong GHG sources, in which case patch identification does not guarantee a GHG hotspot.

3.6 *Implications for field-level emission estimation*

Current practice entails that field-level (model-based) and indeed country-level emission estimates are based on uniform treatments (e.g. N amendments) to specific areas (e.g. Wu et al., 2015; Marsden et al., 2018). This assumes a perfect N distribution and the same response across the rest of the field. However, most GHG source processes are biogenic and highly spatially variable, and this inherent within-field variability in the fluxes is not captured in emission estimates based on fluxes made using chambers. As a result, model-based emissions may be under- or over-estimated. Further, given the underlying flux variability is unknown, any associated uncertainty or confidence in these estimates are similarly poorly constructed (e.g. as found by Shurpali et al. (2016) when diurnal variations are excluded).

Our study provides insight into within-field GHG variability (via the kriging analyses, section 3.2.3) and how soil, topographical and vegetation factors may drive this (via the regression analyses, section 3.3.2) for contrasting extensively and intensively managed pastures. Crucially, this insight is robust through the application of explicitly spatial methods that capture key spatial dependencies in the GHG processes (via the variogram analyses, section 3.2.2), without which false interpretations may result (section 3.3.2). Ultimately, information gained through this and subsequent within-field spatial studies, for all pasture types across all agro-ecological regions should enable the implementation of locally adjusted field-level emission estimates that implicitly acknowledge likely within-field GHG variability, together with associated measures of confidence. Challenges remain in the implementation of such studies and ensuring sufficient sample resolution so that key spatial effects in the GHG processes are captured and how often such studies should be repeated (i.e. ensuring sufficient temporal resolution) to ensure key temporal effects are captured also. Micrometeorological approaches such as eddy covariance can be used alongside chambers to provide better estimates of integrated N_2O emissions for comparison (e.g. Jones et al., 2011).

4. Conclusions

The within-field variability of all three GHGs (N_2O, CO_2, CH_4) at both study sites was high, as expected. The pilot-informed sample design at the Intensive site appeared better able to capture the spatial dependence of fluxes than that found at the Extensive site, highlighting the importance of pilot studies. A REML-based spatial regression was only worth applying to Intensive site N_2O fluxes, which had the strongest spatial dependence of all the gases measured, across both study sites. Importantly, this regression produced a different set of significant predictor variables to that found with an OLS-based regression (from soil moisture, soil NO_3^- and elevation, to soil moisture and bulk density), demonstrating clear value in accounting for spatial effects.

Overall, the significant predictors of the GHG fluxes only exerted a weak consistent influence and were site-specific, suggesting that other factors not recorded in this study may be more important, or relationships were more complex than were captured in the chosen statistical models (e.g. non-linear relationships, models with interacting terms). The strongest regression fit was for Extensive site N_2O with an $R^2 = 0.57$, whose significant predictors, soil NO_3^-, and grassland and marsh vegetation-type could be explained by known N_2O controlling factors and accorded well with the literature. Given the complex balance of factors required to induce emissions of N_2O and CH_4, it is perhaps unsurprising that fluxes are strongly determined by local conditions leading to differences in limiting factors. Changes in the balance of GHG emission-contributors could even change across or within a field leading to more complex relationships between predictors and fluxes, than considered here. In this respect, on-going work is investigating the use of more sophisticated multiscale, GHG spatial regressions that account for non-linear and non-stationary relationships, each operating at their own spatial scale (Murakami et al., 2019).

Acknowledgements

Thanks to Jon Arthur Holmberg, Non Gwenllian Williams, Sian Rowlands, Lucy Greenfield, Maria McMahon and Dave Arnott for their assistance with the Extensive site spatial sampling campaign and sample processing and to Jia Liang, Yang Zhang, Xi Wang and Alison Carswell for assistance with the Intensive site work. Thanks also to Andrew Packwood for vegetation survey information for the Extensive study site.

Funding: This work was supported by the UK Natural Environment Research Council (NERC) [grant numbers NE/M015351/1, NE/M013847/1 and NE/M013154/1]; and by the UK Biotechnology and Biological Sciences Research Council (BBSRC) [grant numbers BBS/E/C/000J0100, BBS/E/C/000I0320 and BBS/E/C/000I0330].

References

Asner, G.P., Elmore, A.J., Olander, L.P., Martin, R.E., Harris, A.T., 2004. Grazing systems, ecosystem responses, and global change. Annu. Rev. of Environ. Resour. 29, 261-99. http://doi.org/10.1146/annurev.energy.29.062403.102142.

Avery, B.W., 1980. Soil Classification for England and Wales (Higher Categories). Soil Surv. Tech. Monogr. No. 14. Harpenden.

Belsley, D.A., Kuh, E., Welsch, R.E., 1980. Regression Diagnostics: Identifying Influential Data and Sources of Collinearity, John Wiley & Sons Inc., Hoboken, New Jersey.

Ball, D.F., 1964. Loss-on-ignition as an estimate of organic matter and organic carbon in non-calcareous soils. J. Soil Sci. 15, 84-92.

Baron, V.S., Dick, A.C., Mapfumo, E., Malhi, S.S., Naeth, M.A., Chanasyk, D.S., 2001. Grazing impacts on soil nitrogen and phosphorus under Parkland pastures. J. Range Manage. 54, 704–710.

797 Betteridge, K., Costall, D., Balladur, S., Upsdell, M., Umemura, K., 2010a. Urine distribution
798 and grazing behaviour of female sheep and cattle grazing a steep New Zealand hill
799 pasture. Anim. Prod. Sci. 50, 624-629. http://doi.org/10.1071/AN09201.
800 Betteridge, K., Hoogendoorn, C., Costall, D., Carter, M., Griffiths, W., 2010b. Sensors for
801 detecting and logging spatial distribution of urine patches of grazing female sheep and
802 cattle. Comput. Electron. Agric. 73, 66-73.
803 http://doi.org/10.1016/j.compag.2010.04.005.
804 Box, G.E.P., Cox, D.R., 1964. An analysis of transforms. J. Royal Stat. Soc. Ser. B
805 (Methodol.). 26, 211-252. https://www.jstor.org/stable/2984418.
806 Brown, P., Cardenas, L., Choudrie, S., Jones, L., Karagianni, E., MacCarthy, J., Passant, N.,
807 Richmond, B., Smith, H., Thistlethwaite, G., Thomson, A., Turtle, L., Wakeling, D.,
808 2020. UK Greenhouse Gas Inventory, 1990 to 2018: Annual Report for submission
809 under the Framework Convention on Climate Change.
810 Butterbach-Bahl, K., Baggs, E.M., Dannenmann, M., Kiese, R., Zechmeister-Boltenstern, S.,
811 2013. Nitrous oxide emissions from soils: how well do we understand the processes and
812 their controls? Philosophical Trans. Royal Soc. B, 368, 20130122.
813 http://doi.org/10.1098/rstb.2013.0122.
814 Cardenas, L.M., Hatch, D.J., Scholefield, D., Jhurreea, D., Clark, I.M., Hirsch, P.R., Salazar,
815 F., Rao-Ravella, S., Alfaro., M., 2013. Potential mineralisation and nitrification in
816 volcanic grassland soils in Chile. Soil Sci. Plant Nutr. 59, 380-391.
817 http://doi.org/10.1080/00380768.2013.789395.
818 Cardenas, L.M., Misselbrook, T.M., Hodgson, C., Donovan, N., Gilhespy, S., Smith, K.A.,
819 Dhanoa, M.S., Chadwick, D., 2016. Effect of the application of cattle urine with or
820 without the nitrification inhibitor DCD, and dung on greenhouse gas emissions from a
821 UK grassland soil. Agric. Ecosyst. Environ. 235, 229–241.

https://doi.org/10.1016/j.agee.2016.10.025.

Chadwick, D.R., Cardenas, L., Misselbrook, T.H., Smith, K.A., Rees, R.M., Watson, C.J., McGeough, K.L, Williams, J.R., Cloy, J.M., Thorman, R.E., Dhanoa, M.S., 2014. Optimizing chamber methods for measuring nitrous oxide emissions from plot-based agricultural experiments. Eur. J. Soil Sci. 65, 295–307. https://doi.org/10.1111/ejss.12117.

Charteris, A.F., Chadwick, D.R., Thorman, R.E., Vallejo, A., de Klein, C.A.M., Rochette, P., Cárdenas, L.M., 2020. Global Research Alliance N2O chamber methodology guidelines: Recommendations for deployment and accounting for sources of variability. J. Environ. Qual. 49, 1092-1109. https://doi.org/10.1002/jeq2.20126.

Chilès, J.-P., Delfiner, P., 1999. Geostatistics: Modelling Spatial Uncertainty, John Wiley & Sons, Hoboken, New Jersey, USA.

Collins, A.L., Burak, E., Harris, P., Pulley, S., Cardenas, L., Tang, Q., 2019. Field scale temporal and spatial variability of $\delta^{13}C$, $\delta^{15}N$, TC and TN soil properties: Implications for sediment source tracing. Geoderma. 333, 108-122. https://doi.org/10.1016/j.geoderma.2018.07.019.

Costa, P.J., 2014. Truncated outlier filtering. J. Biopharm. Stat. 24, 1115-1129. https://doi.org/10.1080/10543406.2014.926366.

Cowan, N.J., Norman, P., Famulari, D., Levy, P.E., Reay, D.S., Skiba, U.M., 2015. Spatial variability and hotspots of soil N_2O fluxes from intensively grazed grassland. Biogeosciences. 12, 1585-1596. http://doi.org/doi:10.5194/bg-12-1585-2015.

De Klein, C.A.M., Harvey. M., 2012. Nitrous oxide chamber methodology guidelines. Global Research Alliance on Agricultural Greenhouse Gases, Ministry for Primary Industries, Wellington, New Zealand.

Decandia, M., Giovanetti, V., Molle, G., Acciaro, M., Mameli, M., Cabiddu, A., Cossu, R.,

Serra, M.G., Manca, C., Rassu, S.P.G, Dimauro, C., 2018. The effect of different time epoch settings on the classification of sheep behaviour using tri-axial accelerometry. Comput. Electron. Agric. 154, 112-119. https://doi.org/10.1016/j.compag.2018.09.002.

Dumortier, P., Aubinet, M., Beckers, Y., Chopin, H., Debacq, A., Gourlez de la Motte, L., Jérôme, E., Wilmus, F., Heinesch, B., 2017. Methane balance of an intensively grazed pasture and estimation of the enteric methane emissions from cattle. Agric. For. Meteorol. 232, 527–535. http://doi.org/10.1016/j.agrformet.2016.09.010.

Duncan, J.M., Groffman, P.M., Band, L.E., 2015. Towards closing the watershed nitrogen budget: Spatial and temporal scaling of denitrification. J. Geophys. Res.: Biogeosciences. 118, 1–15. https://doi.org/10.1002/jgrg.20090.

Evans, J.S., Oakleaf, J., Cushman, S.A., 2014. An ArcGIS Toolbox for surface gradient and geomorphometric modelling. Version 2.0-0. https://github.com/jeffreyevans/GradientMetrics (accessed 06/08/2019).

Fang, C., Moncrieff, J.B., 2001. The dependence of soil CO_2 efflux on temperature. Soil Biol. Biochem. 33, 155-165. https://doi.org/10.1016/S0038-0717(00)00125-5.

FAO (Food and Agriculture Organisation of the United Nations), 1981. Soil Map of the World. UNESCO, Paris.

Flechard, C.R., Ambus, P., Skiba, U., Rees, R.M., Hensen, A., van Amstel, A., van den Pol-van Dasselaar, A., Soussana, J.-F., Jones, M., Clifton-Brown, J., Raschi, A., Horvath, L., Neftel, A., Jocher, M., Ammann, C., Leifeld, J., Fuhrer, J., Calanca, P., Thalman, E., Pilegaard, K., Di Marco, C., Campbell, C., Nemitz, E., Hargreaves, K.J., Levy, P.E., Ball, B.C., Jones, S.K., van de Bulk, W.C.M., Groot, T., Blom, M., Domingues, R., Kasper, G., Allard, V., Ceschia, E., Cellier, P., Laville, P., Henault, C., Bizouard, F., Abdalla, M., Williams, M., Baronti, S., Berretti, F., Grosz, B., 2007. Effects of climate and management intensity on nitrous oxide emissions in grassland systems across

872 Europe. Agric. Ecosyst. Environ. 121, 135–152.
873 https://doi.org/10.1016/j.agee.2006.12.024.
874 Genever, L., Buckingham, S., 2016. Beef and Sheep Better Returns Programme Manual 8:
875 Planning grazing strategies for better returns. Agriculture and Horticulture
876 Development Board (AHDB). http://beefandlamb.ahdb.org.uk/returns/nutrition-and-
877 forage/. Accessed 27/06/2020.
878 Giles, M., Morley, N., Baggs, E.M., Daniell T.J., 2012. Soil nitrate reducing processes –
879 drivers, mechanisms for spatial variation, and significance for nitrous oxide production.
880 Front. Microbiol. 3, 407. http://doi.org/10.3389/fmicb.2012.00407.
881 Giltrap, D.L., Berben, P., Palmada, T., Saggar, S., 2014. Understanding and analysing spatial
882 variability of nitrous oxide emissions from a grazed pasture. Agric. Ecosyst. Environ.
883 186, 1-10. http://doi.org/10.1016/j.agee.2014.01.012.
884 Glastir Entry Booklet 2: Technical Guidance 2015, 2013. Glastir: The new sustainable land
885 management scheme for Wales. Digital ISBN: 978 1 4734 0265 2. WG20573, Welsh
886 Government.
887 Gourlez de la Motte, L. Jérôme, E., Mamadou, O., Beckers, Y., Bodson, B., Heinesch, B.,
888 Aubinet, M., 2016. Carbon balance of an intensively grazed permanent grassland in
889 southern Belgium. Agric. For. Meteorol. 228–229, 370–383.
890 http://doi.org/10.1016/j.agrformet.2016.06.009.
891 Harris, P., 2019. A simulation study on specifying a regression model for spatial data:
892 Choosing between heterogeneity and autocorrelation effects. Geogr. Anal. 51, 151-181.
893 https://doi.org/10.1111/gean.12163.
894 Harrison, A.F., Bocock, K.L., 1981. Estimation of soil bulk-density from loss-on-ignition
895 values. J. Appl. Ecol.18, 919-927.
896 Harrod, T.R., Hogan, D.V., 2008. The soils of North Wyke and Rowden, Revised edition of

original report by Harrod, T.R., 1981. Soil Survey of England and Wales (now the National Soil Resources Institute, Cranfield University, UK). Available from Rothamsted Research. http://resources.rothamsted.ac.uk/farm-platform-national-capability/data-portal-guides-and-information (accessed 05/08/2019).

Hengl, T., Geuvelink, G.B.M., Stein, A., 2003. Comparison of kriging with external drift and regression-kriging. Technical note, International Institute for Geoinformation Science and Earth Observation (ITC), The Netherlands. http://www.itc.nl/library/Papers_2003/misca/hengl_comparison.pdf (accessed 05/08/2019).

Imer, D., Merbold, L., Eugster, W., Buchmann, N., 2013. Temporal and spatial variations of soil CO_2, CH_4 and N_2O fluxes at three differently managed grasslands. Biogeosciences. 10, 5931-5945. http://doi.org/10.5194/bg-10-5931-2013.

Jérôme, E., Beckers, Y., Bodson, B., Heinesch, B., Moureaux, C., Aubinet, M., 2014. Impact of grazing on carbon dioxide exchanges in an intensively managed Belgian grassland. Agric. Ecosyst. Environ. 194, 7–16. http://doi.org/10.1016/j.agee.2014.04.021.

Jolly, B., Saggar, S., Luo, J., Bates, G., Smith, D., Bishop, P., Berben, P., Lindsey, S., 2019. Technologies for mapping cow urine patches: A comparison of thermal imagery, drone imagery, and soil conductivity with Spikey-R, in: Currie, L.D., Christensen C.L. (Eds.), Nutrient loss mitigations for compliance in agriculture. http://flrc.massey.ac.nz/publications.html. Occasional Report No. 32. Fertilizer and Lime Research Centre, Massey University, Palmerston North, New Zealand. 10 pages.

Jones, S.K., Famulari, D., Di Marco, C.F., Nemitz, E., Skiba, U.M., Rees, R.M., Sutton, M.A., 2011. Nitrous oxide emissions from managed grassland: A comparison of eddy covariance and static chamber measurements. Atmos. Meas. Tech. 4, 2179–2194. https://doi.org/10.5194/amt-4-2179-2011.

Kaiser, K.E., McGlynn, B.L., Dore, J.E., 2018. Landscape analysis of soil methane flux across complex terrain. Biogeosciences. 15, 3143–3167. https://doi.org/10.5194/bg-15-3143-2018.

Kazianka, H., Pilz, J., 2010. Copula-based geostatistical modelling of continuous and discrete data including covariates. Stoch. Environ. Res. Risk Assess. 24, 661-673. https://doi.org/10.1007/s00477-009-0353-8.

Klein Goldewijk, K., Beusen, A., Doelman, J., Stehfest, E., 2017. Anthropogenic land use estimates for the Holocene – HYDE 3.2. Earth Syst. Sci. Data. 9, 927-953. https://doi.org/10.5194/essd-9-927-2017.

Kreba, S.A., Coyne, M.S., McCulley, R.L., Wendroth, O.O., 2013. Spatial and temporal patterns of carbon dioxide flux in crop and grass land-use systems. Vadose Zone J. https://doi.org/10.2136/vzj2013.01.0005.

Kronmal, R.A., 1993. Spurious correlation and the fallacy of the ratio standard revisited. J. Royal Stat. Soc. Ser. A (Stat. Soc.). 156, 379-392. https://doi.org/10.2307/2983064.

Liu, S., Herbst, M., Bol, R., Gottselig, N., Pütz, T., Weymann, D., Wiekenkamp, I., Vereecken, H., Brüggemann, N., 2016. The contribution of hydroxylamine content to spatial variability of N_2O formation in soil of a Norway spruce forest. Geochim. Cosmochim. Acta. 178, 76–86. http://doi.org/10.1016/j.gca.2016.01.026.

Lush, L., Wilson, R.P., Holton, M.D., Hopkins, P., Marsden, K.A., Chadwick, D.R., King, A.J., 2018. Classification of sheep urination events using accelerometers to aid improved measurements of livestock contributions to nitrous oxide emissions. Comput. Electron. Agric. 150, 170–177. https://doi.org/10.1016/j.compag.2018.04.018.

Maire, J., Gibson-Poole, S., Cowan, N., Reay, D.S., Richards, K.G., Skiba, U., Rees, R.M., Lanigan, G.J., 2018. Identifying urine patches on intensively managed grassland using aerial imagery captured from remotely piloted aircraft systems. Front. Sustain. Food

947 Syst. 2, 10. https://doi.org/10.3389/fsufs.2018.00010.
948 Marsden, K.A., Holmberg, J.A., Jones, D.L., Chadwick, D.R., 2018. Sheep urine patch N_2O
949 emissions are lower from extensively-managed than intensively-managed grasslands.
950 Agric. Ecosyst. Environ. 265, 264–274. https://doi.org/10.1016/j.agee.2018.06.025.
951 Marsden, K.A., Holmberg, J.A., Jones, D.L., Charteris, A.F., Cárdenas, L.M., Chadwick,
952 D.R., 2019. Nitrification represents the bottle-neck of sheep urine patch N_2O emissions
953 from extensively grazed organic soils. Sci. Total Environ. 695, 133786.
954 https://doi.org/10.1016/j.scitotenv.2019.133786.
955 McClain, M.E., Boyer, E.W., Dent, C.L., Gergel, S.E., Grimm, N.B., Groffman, P.M., Hart,
956 S.C., Harvey, J.W., Johnston, C.A., Mayorga, E., McDowell, W.H., Pinay, G., 2003.
957 Biogeochemical hot spots and hot moments at the interface of terrestrial and aquatic
958 ecosystems. Ecosyst. 6, 301–312, http:// doi.org/10.1007/s10021-003-0161-9.
959 McDaniel, M.D., Simpson, R.G., Malone, B.P., McBratney, A.B., Minasny, B., Adams,
960 M.A., 2017. Quantifying and predicting spatio-temporal variability of soil CH_4 and
961 N_2O fluxes from a seemingly homogeneous Australian agricultural field. Agric.
962 Ecosyst. Environ. 240, 182–193. http://doi.org/10.1016/j.agee.2017.02.017.
963 Met Office. https://www.metoffice.gov.uk/public/weather/climate/gcmnvw66g (accessed:
964 08/12/2018).
965 Moore, I.D., Grayson, R.B., Ladson, A.R., 1991. Digital terrain modelling: A review of
966 hydrological, geomorphological, and biological applications. Hydrol. Process. 5, 3-30.
967 https://doi.org/10.1002/hyp.3360050103.
968 Mudge, P.L., Wallace, D.F., Rutledge, S., Campbell, D.I., Schipper, L.A., Hosking, C.L.,
969 2011. Carbon balance of an intensively grazed temperate pasture in two climatically
970 contrasting years. Agric. Ecosyst. Environ. 144, 271–280.
971 http://doi.org/10.1016/j.agee.2011.09.003.

Murakami, D., Lu, B., Harris, P., Brunsdon, C., Charlton, M., Nakaya, T., Griffith, D., 2019. The importance of scale in spatially varying coefficient modelling. Ann. Assoc. Am. Geogr. 109, 50-70. https://doi.org/10.1080/24694452.2018.1462691.

O'brien, R.M., 2007. A caution regarding rules of thumb for variance inflation factors. Qual. & Quant. 41, 673-690.

Oertel, C., Matschullat, J., Zurba, K., Zimmermann, F., Erasmi, S., 2016. Greenhouse gas emissions from soils—A review, Chem. Erde. 76, 327-352. http://doi.org/10.1016/j.chemer.2016.04.002.

Office for National Statistics (ONS), 2016. UK Natural Capital: Ecosystem accounts for farmland (Experimental Statistics). https://www.ons.gov.uk/economy/environmentalaccounts/bulletins/uknaturalcapital/ecosystemaccountsforfarmlandexperimentalstatistics (accessed 05/08/2019).

Orr, R.J., Murray, P.J., Eyles, C.J., Blackwell, M.S.A., Cardenas, L.M., Collins, A.L., Dungait, J.A.J., Goulding, K.W.T., Griffith, B.A., Gurr, S.J., Harris, P., Hawkins, J.M.B., Misselbrook, T.H., Rawlings, C., Shepherd, A., Sint, H., Tozer, K.N., Wu, L., Lee, M.R.F, 2016. The North Wyke Farm Platform: Effect of temperate grassland farming systems on soil moisture contents, surface run-off and associated water quality dynamics. Eur. J. Soil Sci. 67, 374-385. https://doi.org/10.1111/ejss.12350.

Pardo-Igúzquiza, E., Dowd, P.A., 2005a. Empirical maximum likelihood kriging: The general case. Math. Geol. 37, 477-492. https://doi.org/10.1007/s11004-005-6665-4.

Pardo-Igúzquiza, E., Dowd, P.A., 2005b. EMLK2D: A computer program for spatial estimation using empirical maximum likelihood kriging. Comput. Geosci. 31, 361-370. https://doi.org/10.1016/j.cageo.2004.09.020.

Parkin, T.B., 1993. Spatial variability of microbial processes in soil – A review. J. Environ. Qual. 22, 409-417.

997 Parkin, T.B., Venterea, R.T., 2010. Chapter 3: Chamber-based trace gas flux measurements,
998 in: Follett, R.F. (Eds), Sampling Protocols. United States Department of Agriculture
999 (USDA), pp. 1-39.
1000 https://www.ars.usda.gov/ARSUserFiles/np212/Chapter%203.%20GRACEnet%20Trac
1001 e%20Gas%20Sampling%20Protocols.pdf (accessed 05/08/2019).
1002 Pinheiro, J., Bates, D., DebRoy, S., Sarkar, D., R Core Team, 2019. nlme: Linear and
1003 Nonlinear Mixed Effects Models. R package version 3.1-141. https://CRAN.R-
1004 project.org/package=nlme (accessed 19/08/2019).
1005 Ribeiro Jr., P.J., Diggle, P.J., 2001. geoR: A package for geostatistical analysis. R News. 1,
1006 15-18.
1007 Rodwell, J.S., 2000. British Plant Communities, Cambridge University Press, Cambridge.
1008 Rutledge, S., Mudge, P.L., Campbell, D.I., Woodward, S.L., Goodrich, J.P., Wall, A.M.,
1009 Kirschbaum, M.U.F., Schipper, L.A., 2015. Carbon balance of an intensively grazed
1010 temperate dairy pasture over four years. Agric. Ecosyst. Environ. 206, 10-20,
1011 http://doi.org/10.1016/j.agee.2015.03.011.
1012 Saggar, S., Hedley, C.B., Giltrap, D.L., Lambie, S.M., 2007. Measured and modelled
1013 estimates of nitrous oxide emission and methane consumption from a sheep-grazed
1014 pasture. Agric. Ecosyst. Environ. 122, 357-365.
1015 http://doi.org/10.1016/j.agee.2007.02.006.
1016 Saggar, S., Tate, K.R., Giltrap, D.L., Singh, J., 2008. Soil-atmosphere exchange of nitrous
1017 oxide and methane in New Zealand terrestrial ecosystems and their mitigation options:
1018 A review. Plant Soil. 309, 25–42. http://doi.org/10.1007/s11104-007-9421-3.
1019 Shaw, R., Lark, R.M., Williams, A.P., Chadwick, D.R., Jones, D.L., 2016. Characterising the
1020 within-field scale spatial variation of nitrogen in a grassland soil to inform the efficient
1021 design of in-situ nitrogen sensor networks for precision agriculture. Agric. Ecosyst.

Environ. 230, 294–306. http://doi.org/10.1016/j.agee.2016.06.004.

Shurpali, N., Rannik, Ü., Jokinen, S., Lind, S., Biasi, C., Mammarella, I., Peltola, O., Pihlatie, M., Hyvönen, N., Räty, M., Haapanala, S., Zahniser, M., Virkajärvi, P., Vesala T., Martikainen, P.J. (2016) Neglecting diurnal variations leads to uncertainties in terrestrial nitrous oxide emissions. Sci. Rep. 6, 25739. https://doi.org/10.1038/srep25739.

Sørensen, R., Zinko, U., Seibert, J., 2006. On the calculation of the topographic wetness index: Evaluation of different methods based on field observations. Hydrol. Earth Syst. Sci. 10, 101-112.

Soussana, J.F., Allard, V., Pilegaard, K., Ambus, P., Amman, C., Campbell, C., Ceschia, E., Clifton-Brown, J., Czobel, S., Domingues, R., Flechard, C., Fuhrer, J., Hensen, A., Horvath, L., Jones, M., Kasper, G., Martin, C., Nagy, Z., Neftel, A., Raschi, A., Baronti, S., Rees, R.M., Skiba, U., Stefani, P., Manca, G., Sutton, M., Tuba, Z., Valentini, R., 2007. Full accounting of the greenhouse gas (CO_2, N_2O, CH_4) budget of nine European grassland sites. Agric. Ecosyst. Environ. 121, 121–134. http://doi.org/10.1016/j.agee.2006.12.022.

Takahashi, T., Harris, P., Blackwell, M.S.A., Cardenas, L.M., Collins, A.L., Dungait, J.A.J., Hawkins, J.M.B., Misselbrook, T.H., McAuliffe, G.A., McFadzean, J.N., Murray, P.J., Orr, R.J., Rivero, M.J., Wu, L., Lee, M.R.F., 2018. Roles of instrumented farm-scale trials in trade-off assessments of pasture-based ruminant production systems. Animal. 12, 1766-1776. https://doi.org/10.1017/S1751731118000502.

Turner, D.A., Chen, D., Galbally, I.E., Leuning, R., Edis, R.B., Li, Y., Kelly, K., Phillips, F., 2008. Spatial variability of nitrous oxide emissions from an Australian irrigated dairy pasture. Plant Soil. 309, 77–88. https://doi.org/10.1007/s11104-008-9639-8.

USDA Natural Resources Conservation Service, 2008. Soil quality indicators. Soil Quality

Physical Indicator Information Sheet Series. Bulk Density. https://www.nrcs.usda.gov/wps/portal/nrcs/detail/soils/health/assessment/?cid=stelprdb1237387. Accessed 27/06/2020.

USDA Natural Resources Conservation Service, 2011. Soil quality indicators. Soil Quality Physical Indicator Information Sheet Series. Soil pH. https://www.nrcs.usda.gov/wps/portal/nrcs/detail/soils/health/assessment/?cid=stelprdb1237387. Accessed 27/06/2020.

Velthof, G.L., Jarvis, S.C., Stein, A., Allen, A.G., Oenema, O. 1996. Spatial variability of nitrous oxide fluxes in mown and grazed grasslands on a poorly drained clay soil. Soil Biol. Biochem. 28, 1215-1225.

Webster, R., Lark, M., 2012. Field sampling for environmental science and management, Routledge, London.

Wu, L., Rees, R.M., Tarsitano, D., Zhang, X., Jones, S.K., Whitmore A.P., 2015. Simulation of nitrous oxide emissions at field scale using the SPACSYS model. Sci. Total Environ. 530-531, 76-86, http://dx.doi.org/10.1016/j.scitotenv.2015.05.064.

Zervas, G., Tsiplakou, E., 2012. An assessment of GHG emissions from small ruminants in comparison with GHG emissions from large ruminants and monogastric livestock. Atmos. Environ. 49, 13-23, http://doi.org/10.1016/j.atmosenv.2011.11.039.

Zou, H., Hastie, T., 2005. Regularization and variable selection via the elastic net. J. Royal Stat. Soc. Ser. B (Stat. Methodol.). 67, 301–320.

Figures

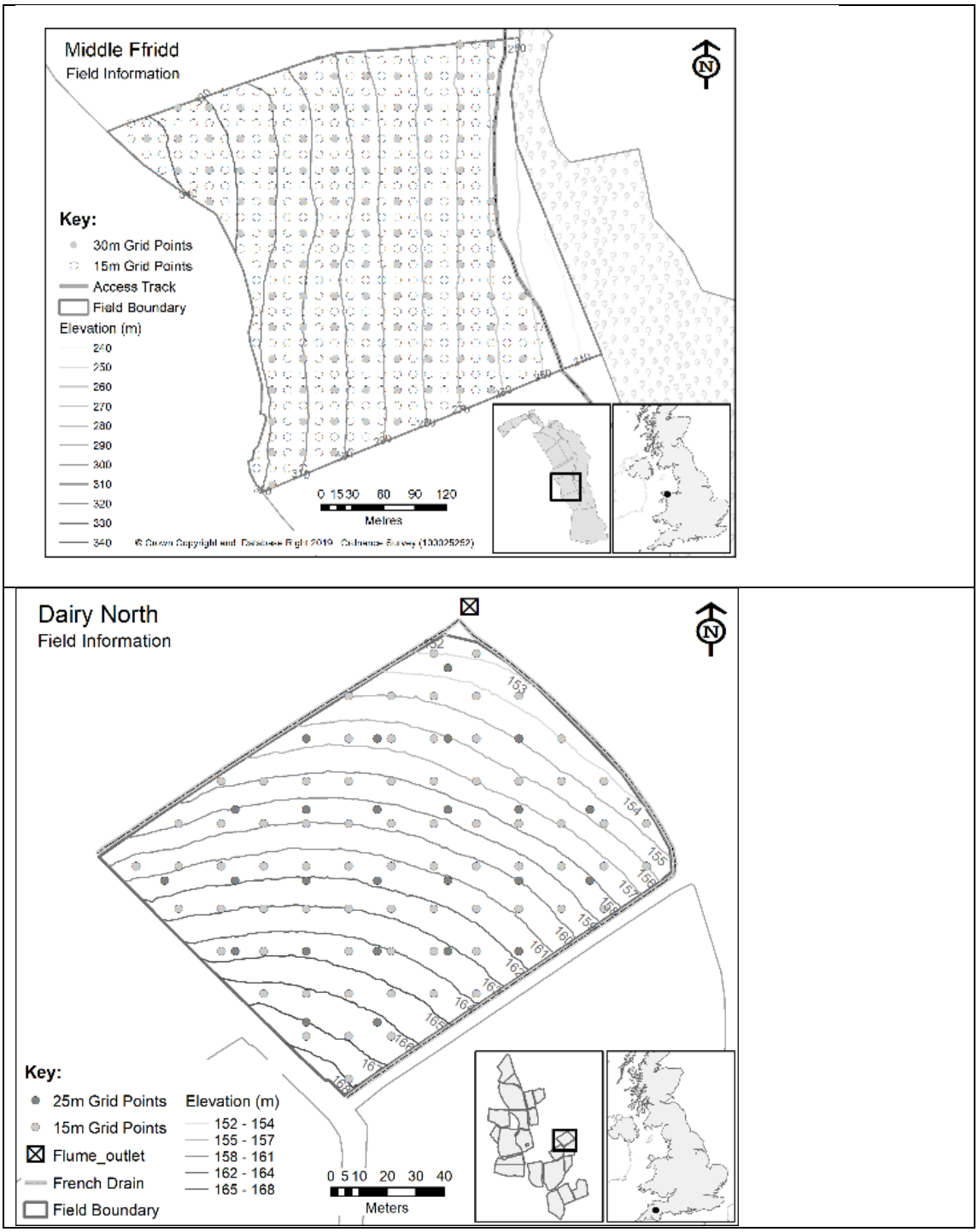

Figure 1

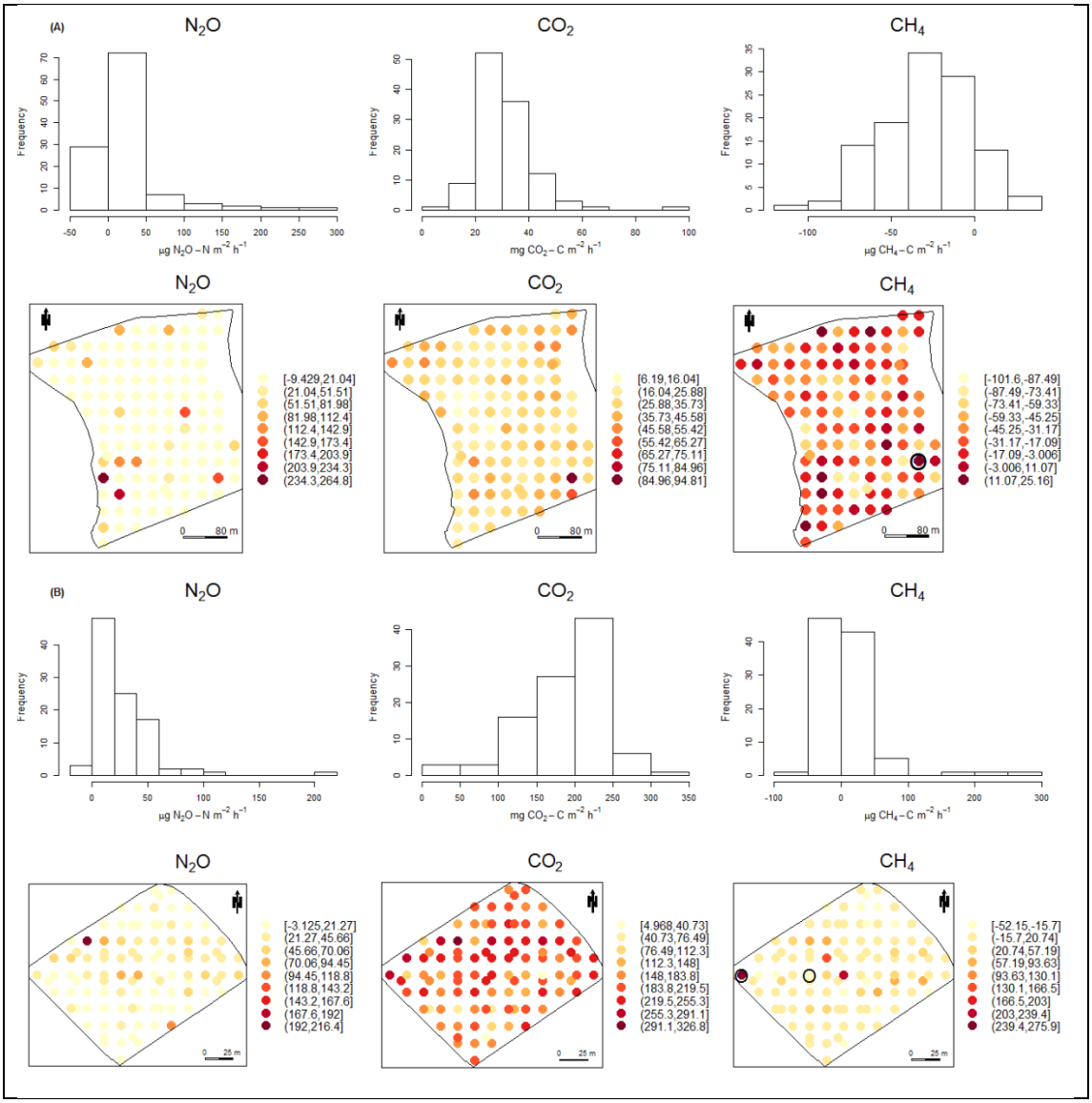
(A)
N2O
CO2
CH4
Frequency
μg N2O – N m−2 h−1
mg CO2 – C m−2 h−1
μg CH4 – C m−2 h−1
[-9.429,21.04]
(21.04,51.51]
(51.51,81.98]
(81.98,112.4]
(112.4,142.9]
(142.9,173.4]
(173.4,203.9]
(203.9,234.3]
(234.3,264.8]
[6.19,16.04]
(16.04,25.88]
(25.88,35.73]
(35.73,45.58]
(45.58,55.42]
(55.42,65.27]
(65.27,75.11]
(75.11,84.96]
(84.96,94.81]
[-101.6,-87.49]
(-87.49,-73.41]
(-73.41,-59.33]
(-59.33,-45.25]
(-45.25,-31.17]
(-31.17,-17.09]
(-17.09,-3.006]
(-3.006,11.07]
(11.07,25.16]
0 80 m
(B)
[-3.125,21.27]
(21.27,45.66]
(45.66,70.06]
(70.06,94.45]
(94.45,118.8]
(118.8,143.2]
(143.2,167.6]
(167.6,192]
(192,216.4]
[4.968,40.73]
(40.73,76.49]
(76.49,112.3]
(112.3,148]
(148,183.8]
(183.8,219.5]
(219.5,255.3]
(255.3,291.1]
(291.1,326.8]
[-52.15,-15.7]
(-15.7,20.74]
(20.74,57.19]
(57.19,93.63]
(93.63,130.1]
(130.1,166.5]
(166.5,203]
(203,239.4]
(239.4,275.9]
0 25 m

Figure 2

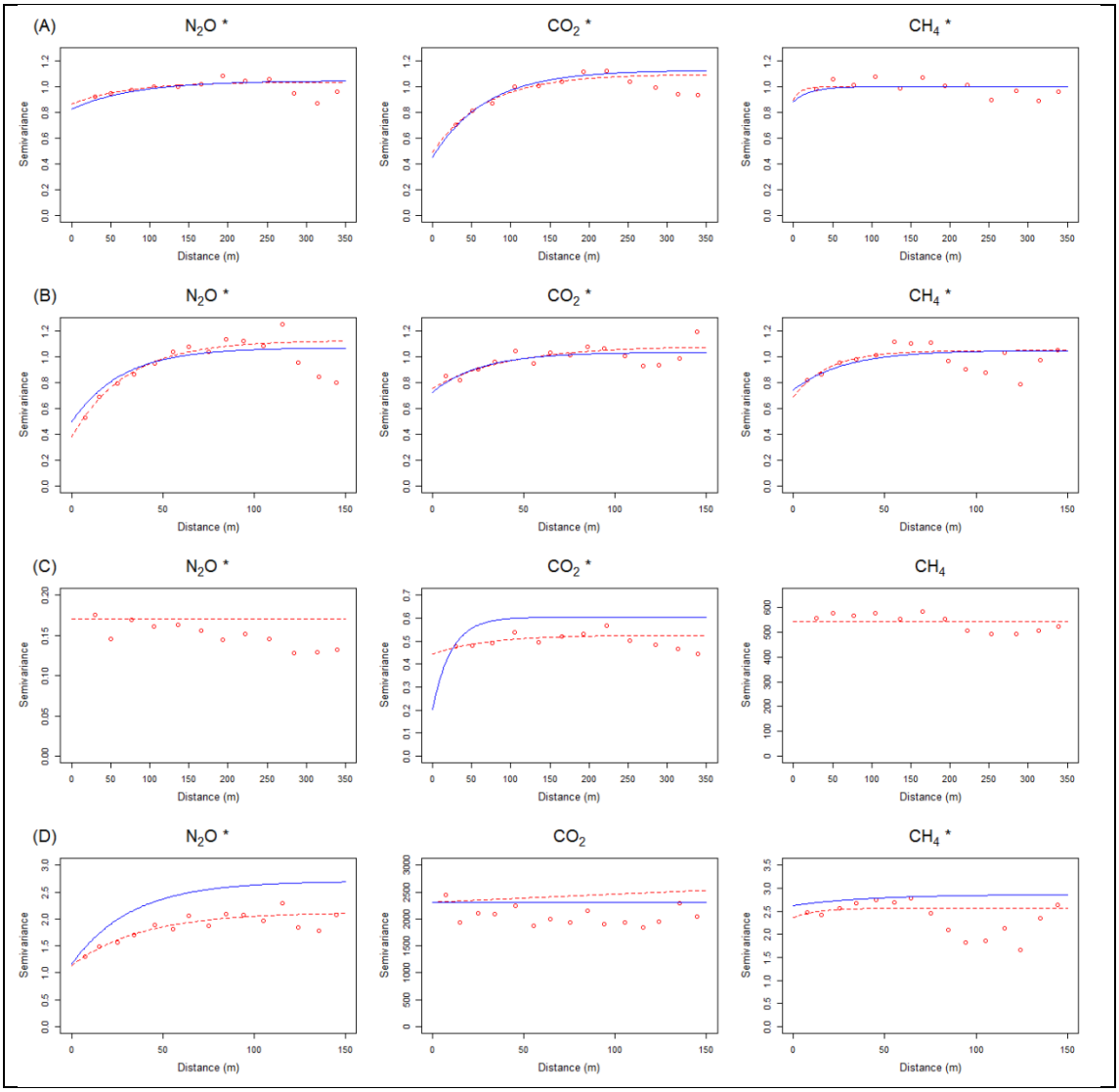
(A)
N_2O *
CO_2 *
CH_4 *
(B)
N_2O *
CO_2 *
CH_4 *
(C)
N_2O *
CO_2 *
CH_4
(D)
N_2O *
CO_2
CH_4 *
Semivariance
Distance (m)

Figure 3

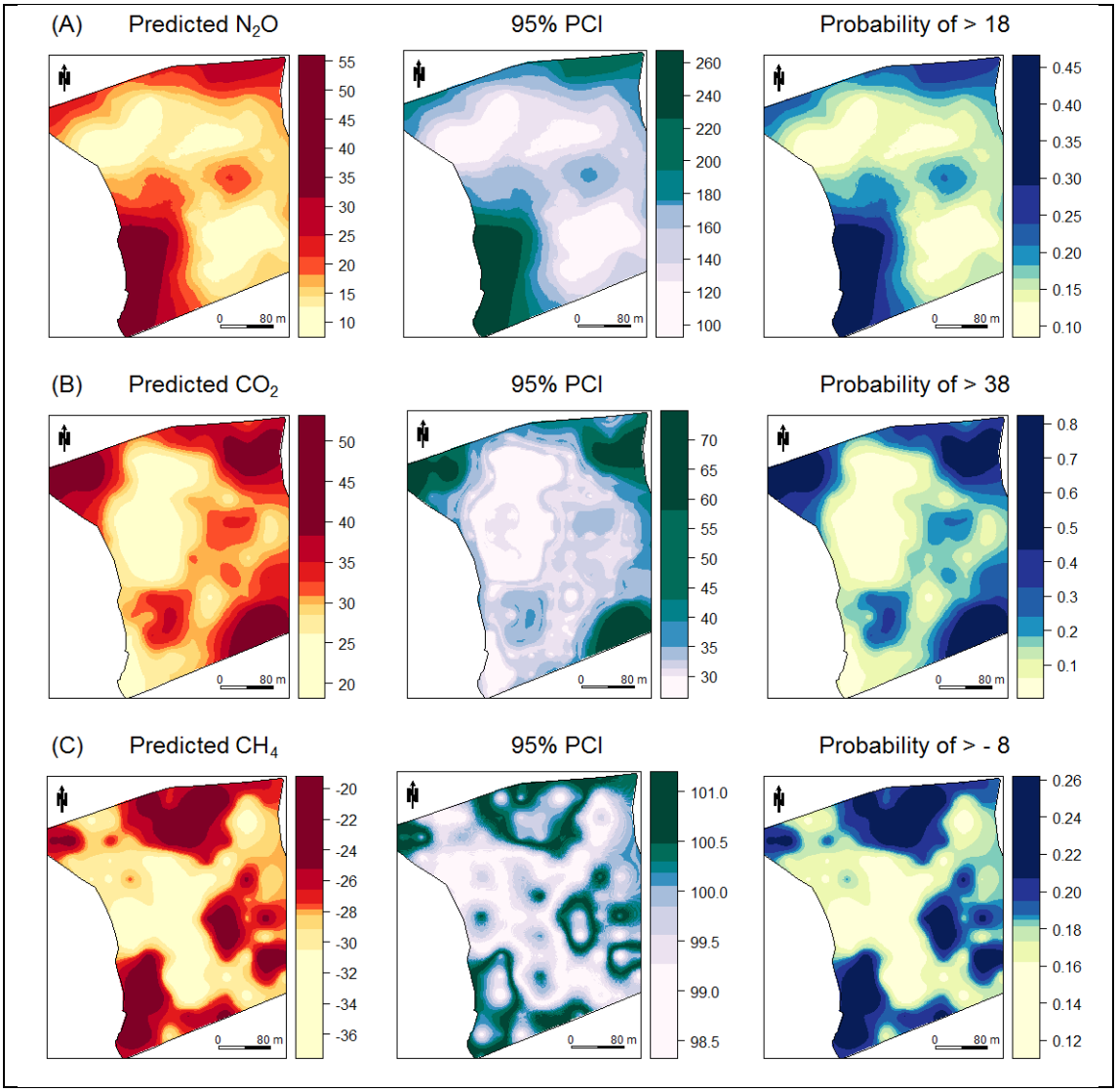
(A) Predicted N_2O
95% PCI
Probability of > 18
55 50 45 40 35 30 25 20 15 10
260 240 220 200 180 160 140 120 100
0.45 0.40 0.35 0.30 0.25 0.20 0.15 0.10
(B) Predicted CO_2
95% PCI
Probability of > 38
50 45 40 35 30 25 20
70 65 60 55 50 45 40 35 30
0.8 0.7 0.6 0.5 0.4 0.3 0.2 0.1
(C) Predicted CH_4
95% PCI
Probability of > - 8
-20 -22 -24 -26 -28 -30 -32 -34 -36
101.0 100.5 100.0 99.5 99.0 98.5
0.26 0.24 0.22 0.20 0.18 0.16 0.14 0.12
0 80 m

Figure 4

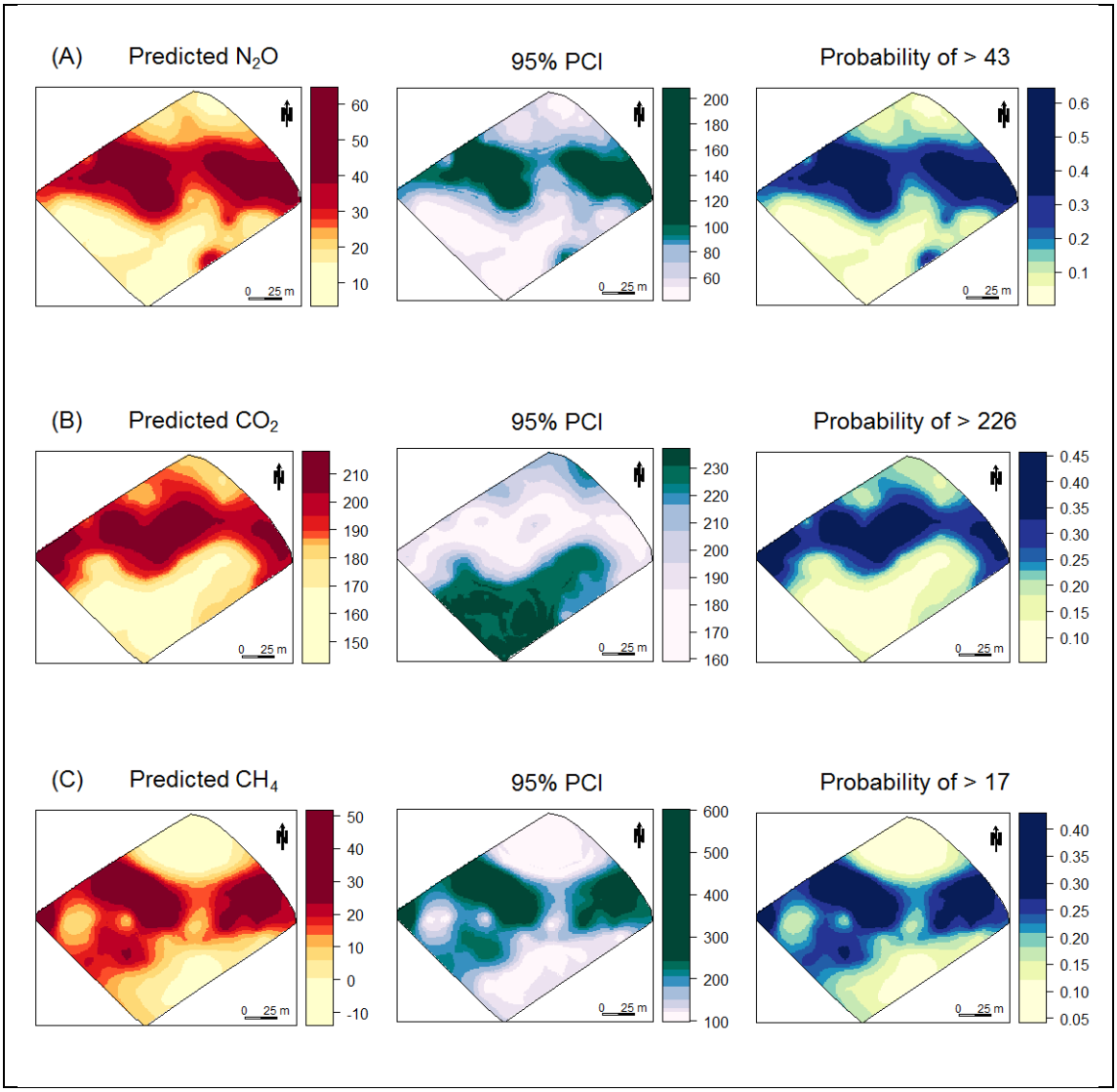
(A) Predicted N_2O
95% PCI
Probability of > 43
(B) Predicted CO_2
95% PCI
Probability of > 226
(C) Predicted CH_4
95% PCI
Probability of > 17
0 25 m

Figure 5

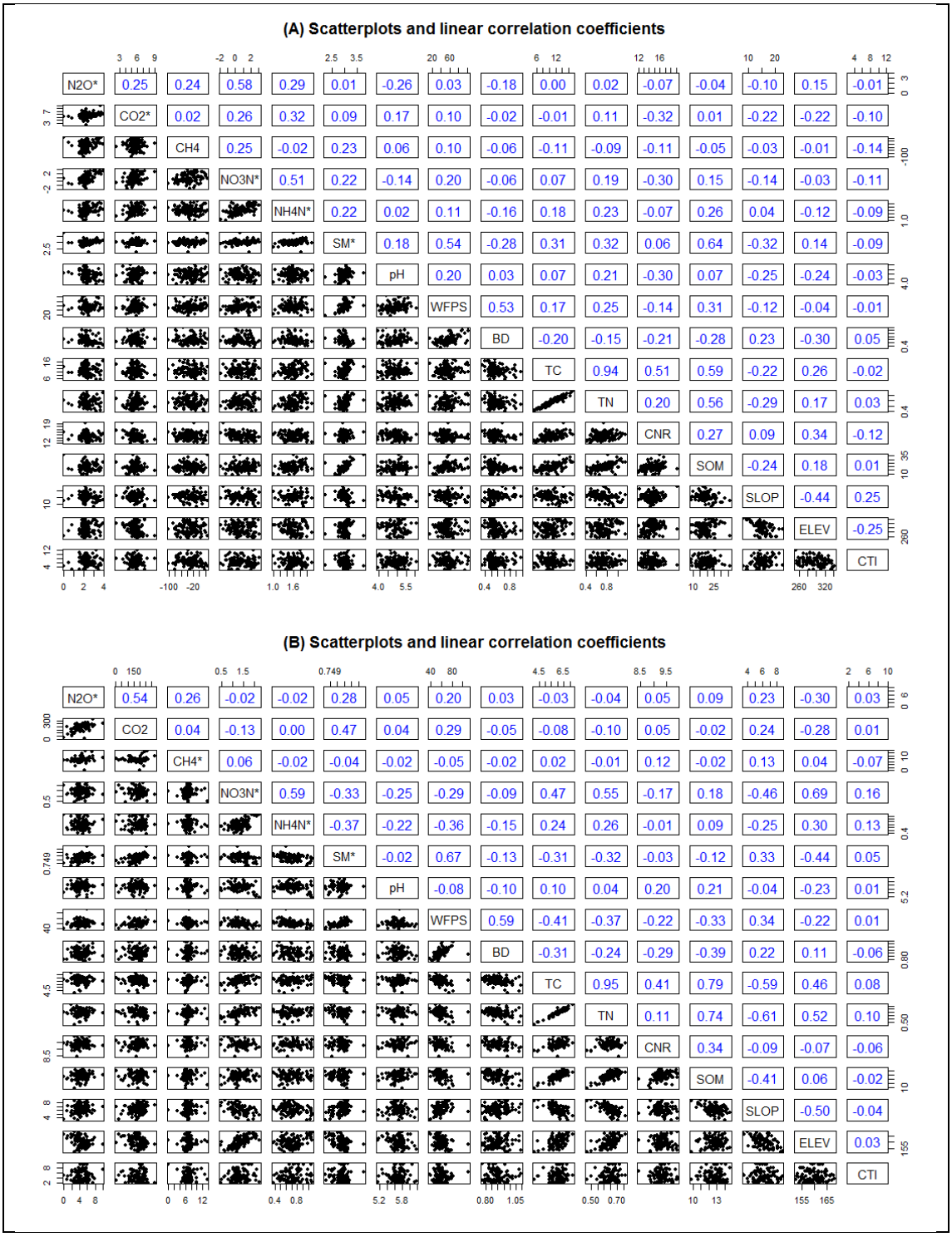
(A) Scatterplots and linear correlation coefficients
N2O* 0.25 0.24 0.58 0.29 0.01 -0.26 0.03 -0.18 0.00 0.02 -0.07 -0.04 -0.10 0.15 -0.01
CO2* 0.02 0.26 0.32 0.09 0.17 0.10 -0.02 -0.01 0.11 -0.32 0.01 -0.22 -0.22 -0.10
CH4 0.25 -0.02 0.23 0.06 0.10 -0.06 -0.11 -0.09 -0.11 -0.05 -0.03 -0.01 -0.14
NO3N* 0.51 0.22 -0.14 0.20 -0.06 0.07 0.19 -0.30 0.15 -0.14 -0.03 -0.11
NH4N* 0.22 0.02 0.11 -0.16 0.18 0.23 -0.07 0.26 0.04 -0.12 -0.09
SM* 0.18 0.54 -0.28 0.31 0.32 0.06 0.64 -0.32 0.14 -0.09
pH 0.20 0.03 0.07 0.21 -0.30 0.07 -0.25 -0.24 -0.03
WFPS 0.53 0.17 0.25 -0.14 0.31 -0.12 -0.04 -0.01
BD -0.20 -0.15 -0.21 -0.28 0.23 -0.30 0.05
TC 0.94 0.51 0.59 -0.22 0.26 -0.02
TN 0.20 0.56 -0.29 0.17 0.03
CNR 0.27 0.09 0.34 -0.12
SOM -0.24 0.18 0.01
SLOP -0.44 0.25
ELEV -0.25
CTI
(B) Scatterplots and linear correlation coefficients
N2O* 0.54 0.26 -0.02 -0.02 0.28 0.05 0.20 0.03 -0.03 -0.04 0.05 0.09 0.23 -0.30 0.03
CO2 0.04 -0.13 0.00 0.47 0.04 0.29 -0.05 -0.08 -0.10 0.05 -0.02 0.24 -0.28 0.01
CH4* 0.06 -0.02 -0.04 -0.02 -0.05 -0.02 0.02 -0.01 0.12 -0.02 0.13 0.04 -0.07
NO3N* 0.59 -0.33 -0.25 -0.29 -0.09 0.47 0.55 -0.17 0.18 -0.46 0.69 0.16
NH4N* -0.37 -0.22 -0.36 -0.15 0.24 0.26 -0.01 0.09 -0.25 0.30 0.13
SM* -0.02 0.67 -0.13 -0.31 -0.32 -0.03 -0.12 0.33 -0.44 0.05
pH -0.08 -0.10 0.10 0.04 0.20 0.21 -0.04 -0.23 0.01
WFPS 0.59 -0.41 -0.37 -0.22 -0.33 0.34 -0.22 0.01
BD -0.31 -0.24 -0.29 -0.39 0.22 0.11 -0.06
TC 0.95 0.41 0.79 -0.59 0.46 0.08
TN 0.11 0.74 -0.61 0.52 0.10
CNR 0.34 -0.09 -0.07 -0.06
SOM -0.41 0.06 -0.02
SLOP -0.50 -0.04
ELEV 0.03
CTI

Figure 6

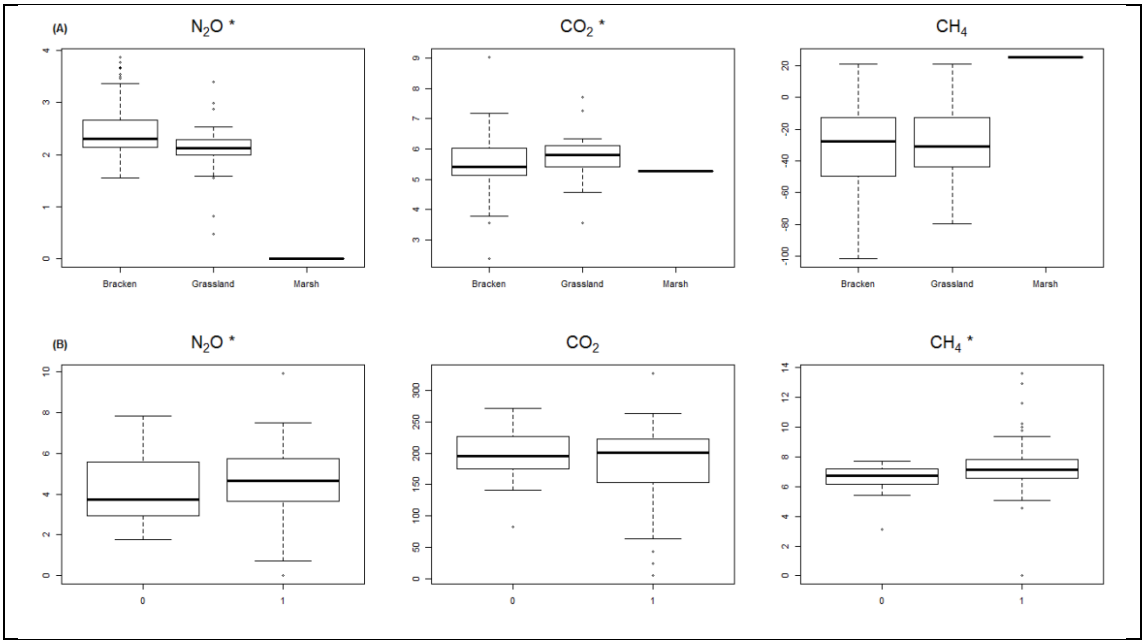

Figure 7

Figure Captions

Figure 1. (A) Extensive (11.5 ha) and (B) Intensive (1.78 ha) sites with sampling locations, both given with field topography.

Figure 2. N_2O, CO_2 and CH_4 histograms and maps for (A) Extensive and (B) Intensive sites. Locations of truncated CH_4 data are shown with "O". Units: μg N_2O-N m^{-2} h^{-1}, mg CO_2-C m^{-2} h^{-1} and μg CH_4-C m^{-2} h^{-1}, respectively.

Figure 3. EMLK variograms for N_2O, CO_2 and CH_4 at (A) Extensive and (B) Intensive sites (all data in normal scores transformed (*) form). LMM residual variograms for N_2O, CO_2 and CH_4 at (C) Extensive and (D) Intensive sites (data in either raw or Box-Cox transformed (*) form). Red points denote empirical variogram, red dashed line denotes WLS variogram model fit to empirical variogram and blue line denotes REML (unbiased) variogram model fit for use in EMLK or the LMM fits, respectively. Residual empirical variograms are found from an OLS regression fit and are biased, as are the WLS variogram model fits.

Figure 4. Extensive site EMLK results for prediction, 95% prediction credible interval (PCI) and risk of exceedance surfaces, for (A) N_2O, (B) CO_2 and (C) CH_4, respectively. Legend class breaks in deciles. Units: μg N_2O-N m^{-2} h^{-1}, mg CO_2-C m^{-2} h^{-1} and μg CH_4-C m^{-2} h^{-1}, respectively.

Figure 5. Intensive site EMLK results for prediction, 95% prediction credible interval (PCI) and risk of exceedance surfaces, for (A) N_2O, (B) CO_2 and (C) CH_4, respectively. Legend class breaks in deciles. Units: μg N_2O-N m^{-2} h^{-1}, mg CO_2-C m^{-2} h^{-1} and μg CH_4-C m^{-2} h^{-1}, respectively.

Figure 6. Scatterplot and correlation coefficient matrices at (A) Extensive and (B) Intensive sites. Data in either raw or Box-Cox transformed (*) form.

Figure 7. Conditional boxplots for N_2O, CO_2 and CH_4 with (A) vegetation-type (VT - for Extensive site) and (B) organic spread (OS - for Intensive site). Data in either raw or Box-Cox

transformed (*) form.

Tables

Table 1: Descriptive statistics of soil parameters and topographical data, expressed on a dry weight basis where applicable (Extensive site n=115; Intensive site n=99).

	Extensive site			**Intensive site**		
	Bulk density (g cm^{-3})	% WFPS (%)	SM θ_g (dry basis; %)	Bulk density (g cm^{-3})	% WFPS (%)	SM θ_g (dry basis; %)
Minimum	0.34	14.9	17.6	0.77	37.9	32.5
Maximum	0.98	103.0	461.5	1.09	111.5	84.6
Mean	0.58	54.5	78.0	0.90	58.8	42.9
Median	0.55	52.2	73.4	0.90	57.1	42.9
Standard error of the mean	0.01	1.6	3.9	0.00	1.0	0.6
Standard Deviation	0.12	16.8	42.0	0.07	10.0	6.1
Qn Scale Estimator	0.09	15.0	19.4	0.06	8.4	4.5
	NO_3^--N (mg kg^{-1})	NH_4^+-N (mg kg^{-1})	pH	NO_3^--N (mg kg^{-1})	NH_4^+-N (mg kg^{-1})	pH
Minimum	0.2	3.5	3.92	1.6	1.6	5.15
Maximum	44.6	102.5	6.07	237.2	146.1	6.18
Mean	5.3	16.2	4.93	14.3	9.7	5.70
Median	2.0	11.4	4.93	6.8	3.1	5.72
Standard error of the mean	0.7	1.3	0.04	2.8	2.3	0.02
Standard Deviation	7.3	13.8	0.44	27.6	22.8	0.18
Qn Scale Estimator	2.0	5.9	0.46	4.5	1.4	0.15
	SOM (%)	% TC	% TN	SOM (%)	% TC	% TN
Minimum	8.7	5.34	0.41	9.8	4.14	0.46
Maximum	36.4	17.40	1.14	14.7	7.24	0.76
Mean	19.2	10.65	0.73	12.8	6.02	0.64
Median	18.7	10.50	0.71	12.9	6.08	0.65
Standard error of the mean	0.5	0.24	0.01	0.1	0.05	0.00
Standard Deviation	4.9	2.60	0.16	1.0	0.53	0.05
Qn Scale Estimator	4.5	2.58	0.16	0.9	0.50	0.05
	Slope (degrees)	Elevation (m asl)	CTI	Slope (degrees)	Elevation (m asl)	CTI
Minimum	8.2	252.3	2.5	3.5	152.8	2.0
Maximum	22.8	342.0	12.1	8.7	167.9	9.7
Mean	15.2	295.5	6.5	6.2	160.1	4.9
Median	15.1	294.8	6.3	6.2	160.0	4.6
Standard error of the mean	0.2	2.2	0.2	0.1	0.4	0.2
Standard Deviation	2.5	23.1	1.9	1.1	3.8	2.1
Qn Scale Estimator	2.2	22.2	1.9	1.1	4.0	2.1

Descriptive statistics for TC:TN were as follows: 12.12, 19.26, 14.50, 14.46, 0.11, 1.23 and 1.24 (Extensive) and 8.44, 9.93, 9.33, 9.30, 0.02, 0.26 and 0.23 (Intensive) for the minimum, maximum, mean, median, standard error of the mean, standard deviation and Qn scale estimator, respectively.

Table 2: Descriptive statistics of GHG fluxes (Extensive site n=115; Intensive site n=99).

	Extensive site			**Intensive site**		
	N_2O	CO_2	CH_4	N_2O	CO_2	CH_4
Minimum	-9.43	6.19	-101.57	-3.12	4.97	-52.14
Maximum	264.80	94.81	25.16	216.42	326.83	275.85
Mean	19.53	31.24	-29.64	27.18	186.49	10.32
Median	4.50	29.42	-28.03	19.17	200.54	0.31
Standard error of the mean	4.10	1.04	2.50	2.84	5.45	4.50
Standard Deviation	43.95	11.22	26.83	28.33	54.24	44.81
Qn Scale Estimator	8.55	8.67	27.54	17.02	47.15	19.42

Units were μg N_2O-N m^{-2} h^{-1}, mg CO_2-C m^{-2} h^{-1} and μg CH_4-C m^{-2} h^{-1}, respectively.

Table 3: REML variogram parameters for N_2O, CO_2 and CH_4, for input into EMLK.

	Extensive site				Intensive site			
GHG/variogram parameter	Nugget variance	Structural variance	Nugget effect	Practical range(m)	Nugget variance	Structural variance	Nugget effect	Practical range(m)
N_2O *	0.825	0.220	0.79	240.0	0.494	0.576	0.46	82.5
CO_2 *	0.451	0.676	0.40	205.2	0.725	0.309	0.70	80.2
CH_4 *	0.882	0.117	0.88	63.8	0.744	0.305	0.71	84.7

Data in normal scores transformed (*) form. The nugget effect is defined as $c_0/c_0 + c_1$, where c_0 is the nugget variance, and c_1 is the structural variance. Ideally, the nugget effect should be as small as possible for a good characterisation of spatial dependence. This table relates to variograms plotted in Figs. 3A, B only.

Table 4: Extensive site non-spatial (OLS) and (if applicable) spatial regression (REML) fits.

Response	**N_2O ***		**CO_2 ***		**CH_4**	
Estimator	**OLS**	**REML**	**OLS**	**REML**	**OLS**	**REML**
Coefficients:						
Intercept	1.9245	-	12.81^{+++}	13.24^{+++}	-191.6	-
NO_3^-N *	0.2860^{+++}	-	-0.02533	0.02883	9.732^{++}	-
NH_4^+N *	0.02430	-	1.144^{++}	0.8687^{+}	-26.42^{+}	-
SM *	0.3560	-	0.3670	-0.07761	46.71^{+}	-
pH	-0.1256	-	-0.3194	-0.2437	9.792	-
BD	-0.4593	-	-0.2503	-0.6876	-21.00	-
TN	-0.4305	-	0.7161	0.6120	-15.51	-
CNR	0.05336	-	-0.1315	-0.1104	0.5481	-
SOM	-0.006213	-	-0.02185	-0.01055	-1.401	-
SLOP	-0.03934	-	-0.1145^{++}	-0.08945^{+}	1.941	-
ELEV	0.0007564	-	-0.01569^{+++}	-0.01443^{++}	0.08796	-
CTI	0.01443	-	-0.04843	-0.04758	-1.058	-
VT (Grassland)	-0.2676^{++}	-	0.3220	0.3000	2.017	-
VT (Marsh)	-2.603^{+++}	-	-0.9276	-0.9824	51.80	-
Variogram parameters:						
Nugget variance	-	-	-	0.204^	-	-
Structural variance	-	-	-	0.400^	-	-
Practical range (m)	-	-	-	71.6^	-	-
OLS/REML fit statistics:					-	
R^2	0.57	-	0.34	0.34	0.25	-
AIC	-	-	315.7	313.6	-	-
BIC	-	-	357.5	358.0	-	-

$^{+++}$, $^{++}$ and $^{+}$ indicate coefficient significantly different to zero at p = 0.001, 0.01 and 0.05 levels, respectively. (*) denotes Box-Cox transformed data. All coefficient estimates given to four significant figures. ^ Variogram parameters were not assessed for significance.

Table 5: Intensive site non-spatial (OLS) and (if applicable) spatial regression (REML) fits.

Response	**N_2O ***		**CO_2**		**CH_4 ***	
Estimator	**OLS**	**REML**	**OLS**	**REML**	**OLS**	**REML**
Coefficients:						
Intercept	-324.0	-433.8^{+}	-25660^{+++}	-	125.8	-
NO_3^-N *	1.652^{+}	1.016	3.265	-	0.9244	-
NH_4^+N *	0.3541	1.396	83.77	-	-1.094	-
SM *	454.4^{+}	597.6^{++}	34160^{+++}	-	-169.8	-
pH	0.3193	0.4253	25.68	-	-0.0005752	-
BD	4.729	6.728^{++}	69.59	-	-1.232	-
TN	4.492	4.373	345.4	-	1.719	-
CNR	0.6829	0.5488	22.08	-	1.088	-
SOM	0.08168	-0.0338	-9.172	-	-0.1882	-
SLOP	0.2538	0.0431	8.243	-	0.3578	-
ELEV	-0.2075^{++}	-0.1812	-2.590	-	-0.01139	-
CTI	-0.02571	-0.0711	-1.516	-	-0.06848	-
OS (1 = inside)	0.5122	0.6069	-5.548	-	0.5891	-
Variogram parameters:						
Nugget variance	-	1.16^	-	-	-	-
Structural variance	-	1.55^	-	-	-	-
Practical range (m)	-	97.7^	-	-	-	-
OLS/REML fit statistics:						-
R^2	0.27	0.27	0.31	-	0.10	-
AIC	360.4	354.2	-	-	-	-
BIC	397.2	396.0	-	-	-	-

$^{+++}$, $^{++}$ and $^{+}$ indicate coefficient significantly different to zero at p = 0.001, 0.01 and 0.05 levels, respectively. (*) denotes Box-Cox transformed data. All coefficient estimates given to four significant figures. ^ Variogram parameters were not assessed for significance.

Supplementary Information

Photographs of the sites:

Supplementary Figure 1. Photograph of the Extensive site taken from the opposite hillside. The darker areas are the bracken stands.

Supplementary Figure 2. Photograph of sheep grazing on the Extensive site.

Supplementary Figure 3. Arial photograph of the Intensive site. Dairy North is the rectangular field in the centre of the image. (Downloaded from the NWFP map site).

Supplementary Figure 4. Photograph of the Intensive site with static chambers in position.

Static chamber designs:

The static chambers used at the Extensive site were made from polyvinyl chloride (PVC) pipe sections (15 cm internal diameter; 25 cm height). Chamber lids (end caps) were manufactured to fit the PVC pipe diameter and modified to include a silicone rubber septum (Suba-Seal®; Sigma, Gillingham, UK) to allow for gas sampling. The end caps pushed into the PVC pipe section forming a seal with gasket foam tape around the upper edge. Cuboid static chambers (40 cm × 40 cm × 25 cm height) were employed at the Intensive site (Cardenas et al., 2016).

Chambers (without their lids) were inserted ca. 5 cm depth into the soil at each sampling point 7-9 days prior to gas sampling at the Extensive site and to a depth of ca. 5 cm or greater (i.e. sufficient to produce an adequate seal) with the aid of a turf-cutter on the day before sampling at the Intensive site.

Gas sampling strategies:

In order to sample the fields rapidly, minimising time differences between sampling points, sampling was conducted by teams of trained researchers (Extensive site, a team of five, sampling 22-24 points each; Intensive site, a team of four, sampling 24-25 points each) following pre-planned sampling routes and standardised sampling protocols.

At the Extensive site, the team started by walking their individual assigned routes and placing chamber lids and gas sample vials next to each chamber. Upon all returning to their starting sample points, GHG sampling commenced (taking place between the hours of 10:40 am and 12:40 pm). Chamber headspaces were mixed by three syringe pumps prior to withdrawing a sample (25 ml) at 0 min and 60 min after chamber lid closure. Supplementary Figure 5 shows an example of a linear increase in headspace N_2O concentrations measured at the Extensive site in autumn 2016. Samples were injected into pre-evacuated 20 ml glass vials. Vials were over-pressurised as a quality control measure, to ensure sample vials had held their seal, (i.e. vials were returned to atmospheric pressure prior to analysis by inserting a syringe and needle, if the syringe plunger pushed back 5 ml it indicated that the vial had held its seal).

At the Intensive site, samples (20 – 22 ml) were withdrawn from the chambers 40 min after lid closure and injected into pre-evacuated 20 ml glass vials. Chamber baseline (0 min) concentrations were approximated by background measurements (n = 10, five before chamber sampling and five after) taken by manually sampling the atmosphere 1 m above the ground around the field (Chadwick et al., 2014). Supplementary Figure 6 shows a few examples of

linear increases in headspace N_2O concentrations measured on different days at the Intensive site in summer 2013.

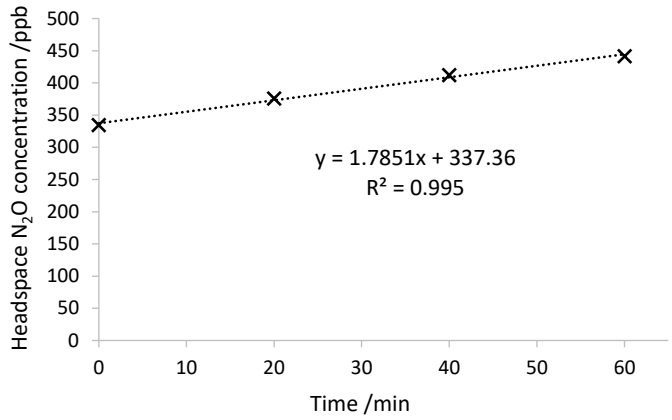

Supplementary Figure 5. Example of linear increase in headspace N_2O concentrations measured at the Extensive site in autumn 2016.

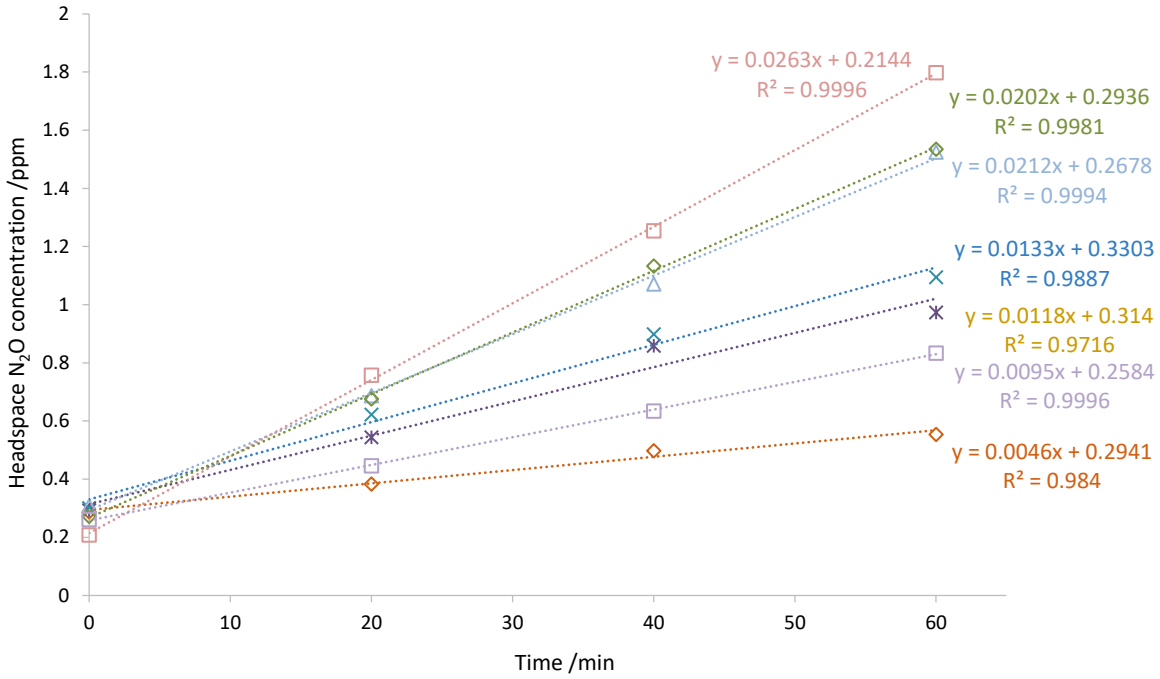

Supplementary Figure 6. Examples of linear increases in headspace N_2O concentrations measured on different days at the Intensive site in summer 2013.

Determination of soil parameters:

Bulk Density and Soil % WFPS

Bulk densities were determined by weighing oven-dried (105 °C; 24 h) and sieved (< 2 mm) soils and accounting for stone and vegetation weight (Extensive site) or volume (Intensive site). Soil % WFPS was calculated by dividing the volumetric water content by the soil porosity. Soil porosity is a function of particle density, which at the Extensive site was determined as a weighted average of the fractions of organic and mineral material, with assumed particle densities of 1.4 g cm^{-3} and 2.65 g cm^{-3}, respectively (Rowell, 1994) due to the higher SOM contents at this site. At the Intensive site a particle density of 2.65 g cm^{-3} was assumed.

Soil extractions and extractable nitrate and ammonium analyses

Soil samples for other analyses were homogenised by hand and large roots and stones removed. Extensive site soil samples were extracted with 0.5 M K_2SO_4 (5 g soil to 25 ml solution) by shaking for 30 min (200 rev min^{-1}), centrifuging (10 000 *g*) and recovering the supernatant. Intensive site soil samples were sieved to 6 mm prior to extraction with 2 M KCl (50 g soil to 100 ml extractant), by shaking for 60 min (150 strokes min^{-1}) and filtering extracts through rinsed high purity filter papers. Both are standard methods, which are considered comparable (Jones and Willett, 2006).

Extensive site soil extracts were analysed for extractable-NO_3^- and NH_4^+ via the colorimetric methods of Miranda et al. (2001) and Mulvaney (1996) using a microplate reader. Intensive site soil extracts were analysed using an Aquakem 250 (Thermo Fisher Scientific Ltd.), a discrete photometric analyser. Extractable total oxidised nitrogen concentrations were determined as nitrite (NO_2^-) via reduction of NO_3^- to NO_2^- by vanadium chloride and a version of the Griess reaction. As soil NO_2^- concentrations are generally very low, measured extractable total oxidised nitrogen concentrations have been assumed to be equivalent to extractable soil NO_3^- concentrations. Extractable NH_4^+ concentrations were determined by reaction to an indophenol via a modified version of the Berthelot reaction (Krom, 1980; Searle, 1984).

Soil pH

Soil pH was measured on fresh Extensive site soils (5 g to 12.5 ml distilled water; briefly shaken and allowed to settle) using standard electrodes. For the Intensive site, soil pH was determined on 10 ml air-dried, ground and sieved (< 2 mm) soil shaken (15 min) in 25 ml deionised water (MAFF 427, 1986) using a Jenway 3320 pH meter (Jenway Ltd., Felsted, Essex, UK).

Soil moisture and soil organic matter

Gravimetric soil moisture contents of all soil samples (ca. 4 g fresh soil for the Extensive site, 20 g for the Intensive site) were determined by mass loss during oven drying (105 °C; 24 h). Soil organic matter contents were determined via loss-on-ignition (ca. 2 g oven-dried soil for the Extensive site; 10 g for the Intensive site) in a muffle furnace (450 °C, 16 h for the Extensive site (Ball, 1964); 400 °C, overnight for the Intensive site (Davies, 1974; Ben-Dor and Banin, 1989; Schulte et al., 1991)).

Total C and N analyses

For the Extensive site, total soil C and soil N content were determined on oven-dried and ground soils using a TruSpec® Analyzer (Leco Corp., St. Joseph, MI). For the Intensive site, total soil C and N content were determined on sieved (< 2 mm), oven-dried (105 °C, 24 h) and ground soils using a Carlo Erba NA2000 elemental analyser (Fisons instruments) coupled to a PDZ Europa 20-22 isotope ratio mass spectrometer (Sercon Ltd., Cheshire, UK). Weighed samples (to achieve 8-3500 µg C and 0.5-215 µg N), sealed in tin capsules, were combusted in a chromium oxide packed tube under oxygen (O_2) and products carried in helium (He) over heated copper wires to reduce N oxides to N_2 and remove excess O_2. Water was removed by a magnesium perchlorate trap and N_2 and CO_2 were chromatographically separated and quantified in the mass spectrometer.

Determination of gas parameters:

Soil headspace N_2O, CO_2 and CH_4, concentrations were determined using the same Perkin Elmer Clarus 580 Gas Chromatograph, served with a Turbo Matrix 110 auto-sampler (Perkin Elmer Inc., Beverly, CT) for samples from both sites. The gas samples passed through two Elite-Q mega bore columns via a split injector, with one connected to an electron capture detector at 375 °C for N_2O measurement and the other to a flame ionisation detector for CO_2 and CH_4 determination. The oven temperature of the gas chromatograph was maintained at 50 °C and oxygen free nitrogen (OFN; BOC, UK) was used as the carrier gas. Soil GHG fluxes were calculated using the increase in headspace N_2O, CO_2 and CH_4 concentrations between 0 min and 60 min (Extensive) or 0 min and 40 min (Intensive). Intensive site gas samples were

run within 24 h of collection.

Topographic data:

Elevation, aspect and slope data were calculated from 1 m LiDAR grids using the Spatial Analyst extension within ArcMap 10.4.1, where values for the sample point locations were obtained using the ArcMap Extraction toolset. At the Extensive site, the 1 m LiDAR grid was created by the Environment Agency Geomatics group and subsequently distributed by Natural Resources Wales. At the Intensive site, the 1 m LiDAR grid was created by the Tellus South West project.

Empirical Maximum Likelihood Kriging (EMLK):

EMLK is a sophisticated kriging algorithm where more efficient results (over a standard kriging algorithm) are obtained by solving the prediction problem in the Gaussian domain via a normal scores transform of the sample data. A Bayesian component in EMLK ensures conditionally unbiased results where a posterior predictive distribution is found at all target locations $\boldsymbol{s}$ (in this study, a grid). For a variable z, the mean of the posterior distribution is taken as the EMLK prediction $\hat{z}_{EMLK}(\boldsymbol{s})$ and the variance of the posterior distribution ${\sigma^2}_{EMLK}(\boldsymbol{s})$ can be used to assess the uncertainty of $\hat{z}_{EMLK}(\boldsymbol{s})$. In all six study kriging runs, isotropic exponential variogram models (e.g. Chilès and Delfiner, 1999) were chosen to characterise the spatial dependence in the normal scores data sets of the N_2O, CO_2 and CH_4 fluxes. EMLK was chosen to predict the GHG data, in so much it is: (i) advocated for small data sets; (ii) advocated for non-normal data sets, including those with observations below the limit of detection; (iii) able (via its Bayesian construction) to provide a more realistic approach to prediction uncertainty than that found in many standard kriging algorithms (e.g. see discussions given in Harris et al., 2010) and, in turn, can provide reliable estimates of risk for exceeding a given GHG emission threshold; and (iv) it is open-source (FORTRAN code, EMLK2D.FOR). Applications of EMLK to soil data can be found in Pardo-Igúzquiza and Chica-Olmo (2005); Radu et al. (2013); Glennon et al. (2014).

SI references

Ball, D.F., 1964. Loss-on-ignition as an estimate of organic matter and organic carbon in non-

calcareous soil. J. Soil Sci. 15, 84-92. https://doi.org/10.1111/j.1365-2389.1964.tb00247.x.

Ben-Dor, E., Banin, A., 1989. Determination of organic matter content in arid-zone soils using a simple 'loss-on-ignition' method. Commun. Soil Sci. Plant Anal. 20, 1675–1695. https://doi.org/10.1080/00103628909368175.

Cardenas, L.M., Misselbrook, T.M., Hodgson, C., Donovan, N., Gilhespy, S., Smith, K.A., Dhanoa, M.S., Chadwick, D., 2016. Effect of the application of cattle urine with or without the nitrification inhibitor DCD, and dung on greenhouse gas emissions from a UK grassland soil. Agric. Ecosyst. Environ. 235, 229–241. https://doi.org/10.1016/j.agee.2016.10.025.

Chadwick, D.R., Cardenas, L., Misselbrook, T.H., Smith, K.A., Rees, R.M., Watson, C.J., McGeough, K.L, Williams, J.R., Cloy, J.M., Thorman, R.E., Dhanoa, M.S., 2014. Optimizing chamber methods for measuring nitrous oxide emissions from plot-based agricultural experiments. Eur. J. Soil Sci. 65, 295–307. https://doi.org/10.1111/ejss.12117.

Chilès, J.-P., Delfiner, P., 1999. Geostatistics: Modelling Spatial Uncertainty, John Wiley & Sons, Hoboken, New Jersey, USA.

Davies, B.E., 1974. Loss-on-ignition as an estimate of soil organic matter. Soil Sci. Soc. Am. J. 38, 150–151. https://doi.org/10.2136/sssaj1974.03615995003800010046x.

Glennon, M., Harris, P., Finne, T., Scanlon, R., O'Connor, P., 2014. The Dublin SURGE Project: Geochemical baseline for heavy metals in topsoils and spatial correlation with historical industry in Dublin, Ireland. Environ. Geochem. Health. 36, 235-254. https://doi.org/10.1007/s10653-013-9561-8.

Harris, P., Charlton, M., Fotheringham, A.S., 2010. Moving window kriging with geographically weighted variograms. Stoch. Environ. Res. Risk Assess. 24, 1193-1209. https://doi.org/10.1007/s00477-010-0391-2.

Jones, D.L., Willett, V.B., 2006. Experimental evaluation of methods to quantify dissolved organic nitrogen (DON) and dissolved organic carbon (DOC) in soil. Soil Biol. Biochem. 38, 991-999. https://doi.org/10.1016/j.soilbio.2005.08.012.

Krom, M.D., 1980. Spectrophotometric determination of ammonia: A study of a modified Berthelot reaction using salicylate and dichloroisocyanurate. The Analyst. 105, 305-316.

MAFF (Ministry of Agriculture, Fisheries and Food) reference book 427, 1986. The analysis of agricultural materials – Method 32: pH and Lime requirement of Mineral Soil.

Miranda, K.M., Epsey, M.G., Wink, D.A., 2001. A rapid, simple, spectrophotometric method for simultaneous detection of nitrate and nitrite. Nitric Oxide. 5, 62-71.

https://doi.org/10.1006/niox.2000.0319.

Mulvaney, R.L., 1996. Nitrogen – inorganic forms, in: Sparks, D.L. (Eds.), Methods of Soil Analysis, Part 3. Soil Science Society of America Inc., Madison, WI, USA, pp. 1123-1184.

Pardo-Igúzquiza, E., Chica-Olmo, M., 2005. Interpolation and mapping of probabilities for geochemical variables exhibiting spatial intermittency. Appl. Geochem. 20, 157-168. https://doi.org/10.1016/j.apgeochem.2004.05.007.

Radu, T., Gallagher, S., Byrne, B., Harris, P., Coveney, S., McCarron, S., McCarthy, T., Diamond, D., 2013. Portable X-Ray Fluorescence as a rapid technique for surveying elemental distributions in soil. Spectrosc. Lett. 46, 516-526. https://doi.org/10.1080/00387010.2013.763829.

Rowell, D.L., 1994. Soil Science: Methods and applications, Routledge, New York, USA.

Searle, P.L., 1984. The Berthelot or indophenol reaction and its use in the analytical chemistry of nitrogen: A review, Analyst. 109, 549-568. https://doi.org/10.1039/AN9840900549.

Schulte, E.E., Kaufmann, C., Peter, J.B., 1991. The influence of sample size and heating time on soil weight loss-on-ignition. Commun. Soil Sci. Plant Anal. 22, 159–168. https://doi.org/10.1080/00103629109368402.